HIPPOCAMPUS 24:1430–1448 (2014)

Intrinsic Mechanisms Stabilize Encoding and Retrieval Circuits Differentially in a Hippocampal Network Model

Ali Hummos,[1,2] Charles C. Franklin,[3] and Satish S. Nair[3]*

ABSTRACT: Acetylcholine regulates memory encoding and retrieval by inducing the hippocampus to switch between pattern separation and pattern completion modes. However, both processes can introduce significant variations in the level of network activity and potentially cause a seizure-like spread of excitation. Thus, mechanisms that keep network excitation within certain bounds are necessary to prevent such instability. We developed a biologically realistic computational model of the hippocampus to investigate potential intrinsic mechanisms that might stabilize the network dynamics during encoding and retrieval. The model was developed by matching experimental data, including neuronal behavior, synaptic current dynamics, network spatial connectivity patterns, and short-term synaptic plasticity. Furthermore, it was constrained to perform pattern completion and separation under the effects of acetylcholine. The model was then used to investigate the role of short-term synaptic depression at the recurrent synapses in CA3, and inhibition by basket cell (BC) interneurons and oriens lacunosum-moleculare (OLM) interneurons in stabilizing these processes. Results showed that when CA3 was considered in isolation, inhibition solely by BCs was not sufficient to control instability. However, both inhibition by OLM cells and short-term depression at the recurrent CA3 connections stabilized the network activity. In the larger network including the dentate gyrus, the model suggested that OLM inhibition could control the network during high cholinergic levels while depressing synapses at the recurrent CA3 connections were important during low cholinergic states. Our results demonstrate that short-term plasticity is a critical property of the network that enhances its robustness. Furthermore, simulations suggested that the low and high cholinergic states can each produce runaway excitation through unique mechanisms and different pathologies. Future studies aimed at elucidating the circuit mechanisms of epilepsy could benefit from considering the two modulatory states separately. © 2014 Wiley Periodicals, Inc.

KEY WORDS: Pattern separation and completion; biologically realistic model; acetylcholine; seizures; interneurons

INTRODUCTION

The hippocampus plays an important role in memory storage and retrieval. Through the process of pattern completion, the CA3 region of the hippocampus aids in the retrieval of previously learned memory traces even from partial cues or noisy inputs (Marr, 1971). In contrast, the dentate gyrus (DG) functions to separate neural representations of similar memories (pattern separation), via a different circuit, to optimize their storage and later retrieval (Marr, 1971; for review, see Hunsaker and Kesner, 2013).

The recurrent connections in the hippocampal CA3 region are implicated in the retrieval of memories (Marr, 1971). However, it is also known that networks with high levels of recurrence are inherently unstable (Marr, 1971; Miles and Wong, 1983, 1987; Cossart et al., 2005; Beyeler et al., 2013). Excitatory activity in CA3 can be amplified and propagated throughout the network, creating a seizure-like response.

Furthermore, projections from DG to CA3 through the mossy fibers (MFs) can also result in runaway excitation (Lawrence and McBain, 2003). Acetylcholine (ACh) has been proposed as a regulator of the circuit with high levels favoring pattern separation, and low levels facilitating pattern completion (Hasselmo et al., 1995). The neuromodulator ACh has a prominent role in encoding new memories and high cholinergic levels are induced by novelty and active exploration (Barry et al., 2012). It alters the circuit dynamics by lowering the synaptic efficacy at the recurrent connections in CA3 and by boosting transmission at MF synapses from DG to CA3. This combination, together with other effects on synapses and cell excitability, allows the network to encode separated representations of the current input while reducing interference from previously encoded memories (Hasselmo et al., 1995). These separated neuronal representations of memories are created in DG and subsequently transmitted to CA3 through the sparse but powerful MFs (Henze et al., 2002). Therefore, though the recurrent connections are suppressed during encoding, the impinging current from DG through these "detonator" synapses can also destabilize the CA3 network (Lawrence and McBain, 2003).

Computational models of pattern separation and completion in the hippocampus have provided an important conceptual framework of how these processes might be regulated in the hippocampus (Treves and Rolls, 1992; Hasselmo et al., 1995) and have been validated experimentally (Rolls and Kesner,

[1] **Department of Health Informatics, University of Missouri, Columbia, Missouri;** [2] **Department of Psychiatry, University of Missouri, Columbia, Missouri;** [3] **Department of Electrical & Computer Engineering, University of Missouri, Columbia, Missouri**

Additional Supporting Information may be found in the online version of this article.

Grant sponsor: NIMH; Grant number: MH087755 (to SSN).

*Correspondence to: Satish S. Nair, Department of Electrical & Computer Engineering, University of Missouri, 229 Engineering Building West, Columbia, MO 65211. E-mail: NairS@Missouri.edu

Accepted for publication 16 June 2014.
DOI 10.1002/hipo.22324
Published online 30 June 2014 in Wiley Online Library (wileyonlinelibrary.com).

2006; Leutgeb et al., 2007; Neunuebel and Knierim, 2014). Recent models have extended these results using spiking neurons (Meeter et al., 2004; Nolan et al., 2010). These models focused on the mechanisms and dynamics of memory storage and retrieval, and handled the instability in the network indirectly using a number of techniques such as normalizing total network activity (Treves and Rolls, 1992), using abstract models of feedback inhibition and attractor dynamics (Hasselmo et al., 1995), explicitly limiting the number of active cells (Meeter et al., 2004), and excluding recurrent connections from the model (Nolan et al., 2010).

In the present study, we explicitly focus on intrinsic hippocampal mechanisms such as short-term plasticity (Abbott and Nelson, 2000), and interneurons (Lawrence and McBain, 2003), to investigate their roles in controlling neuronal excitability and the pathological states they might engender. Toward this end, we developed a biologically realistic model of the hippocampus that included principal cells and two of the most common interneurons, basket cells (BCs) and oriens lacunosum-moleculare (OLM) cells (Vida, 2010). Both interneuron types are well studied and are differentially modulated by ACh (Lawrence et al., 2006). We matched experimentally reported behaviors, including neuronal excitability, synaptic current dynamics, network spatial connectivity patterns, and short-term synaptic plasticity. The model suggested that OLM and BC inhibition and short-term synaptic plasticity contribute differently to network stability. Additionally, pattern separation and completion circuits in the hippocampus might produce instability through different dynamics, consequently requiring different mechanisms for their stabilization.

METHODS

We developed a biologically realistic network model of the hippocampus that included networks for entorhinal cortex (EC), DG, and CA3 regions. The model is described next with the mathematical details and additional experimental data used provided in Supporting Information. The model was implemented using the NEURON software package (Carnevale and Hines, 2009). The code will be made available upon publication via the ModelDB public database (http://senselab.med.yale.edu/ModelDB/).

Single Cell Models

The model cells in CA3 were pyramidal cells and two of the most abundant interneuron types, BC and OLM cells (Vida, 2010). The model cells in DG were granule cells, BC, and Hilar Perforant Path-associated (HIPP) cells.

Single neurons were modeled using the Izhikevich formulation (2003, 2010). This formulation provides a reduced-order model that preserves many of the neurocomputational properties of more detailed biological models. We provide an overview below on how model neurons were matched to the salient features of electrophysiological recordings (Fig. 1). Section S2 in Supporting Information has further experimental data considered in developing the single cell models, and a listing of the model equations and parameters used.

For CA3 pyramidal cells, the resting membrane potential was set to -75 mv, spike threshold to -53 mv, and peak action potential voltage to 29 mv, as reported by Brown and Randall (2009). The remaining cell model parameters were tuned to match responses to both long and short current injections (Fig. 1, Supporting Information Table S1; Brown and Randall, 2009). Similarly, in developing the DG granule cells model, resting membrane potential, threshold, and peak action potential were set using data from Staley et al. (1992) and the model was then tuned to match current injection responses (Fig. 1, Supporting Information Table S1; Staley et al., 1992). OLM model passive properties were estimated from Ali and Thompson (1998), and the behavior of the cells was matched to current injections from the same study. In particular, we matched the spike frequency adaptation, the prominent slow after-hyperpolarization potential (AHP, Fig. 1), sag response, and rebound spikes (Supporting Information Fig. S1). For BC model, membrane properties (Supporting Information Table S1), current injection responses (Fig. 1), and finally current vs. firing rate relationship (Supporting Information Fig. S2) were matched to data reported by Buhl et al. (1996). Due to the striking similarity of OLM and HIPP cells (Katona et al., 1999), we used the same model for both cell types.

Neurons in the model had membrane potential values drawn from a random distribution. The initial voltage was drawn from a normal distribution with a mean 5 mv lower than their resting potential, and with a standard deviation of 10 mv. These values maintained the network stability at the beginning of simulations.

Network Structure and Connectivity

The rat hippocampus contains $\sim$1.6 million cells (Hosseini-Sharifabad and Nyengaard, 2007). For computational efficiency, the numbers were scaled down while maintaining reported ratios (see Section S3.1 of Supporting Information). The model DG region had 384 granule cells, and 32 each of BC and HIPP interneurons, while the model CA3 region contained 63 pyramidal cells and 8 each of BC and OLM interneurons (Seress and Pokorny, 1981; Kosaka et al., 1987; Baude et al., 2007; Hosseini-Sharifabad and Nyengaard, 2007).

The EC provides inputs to the hippocampus through the perforant pathway that projects to the entire hippocampal formation. The standard view describes a unidirectional connectivity with a direct pathway from EC to CA3 and an indirect pathway through DG (Fig. 2A,B; Naber et al., 1997; Witter, 2010). The perforant path projections follow a lamellar organization across the longitudinal axis of the hippocampus, as follows: lateral and posterior parts of the EC are connected to the dorsal parts of CA3 and DG, while the medial and anterior parts of EC project to the ventral parts of CA3 and DG. This lamellar organization transitions gradually from one extreme to

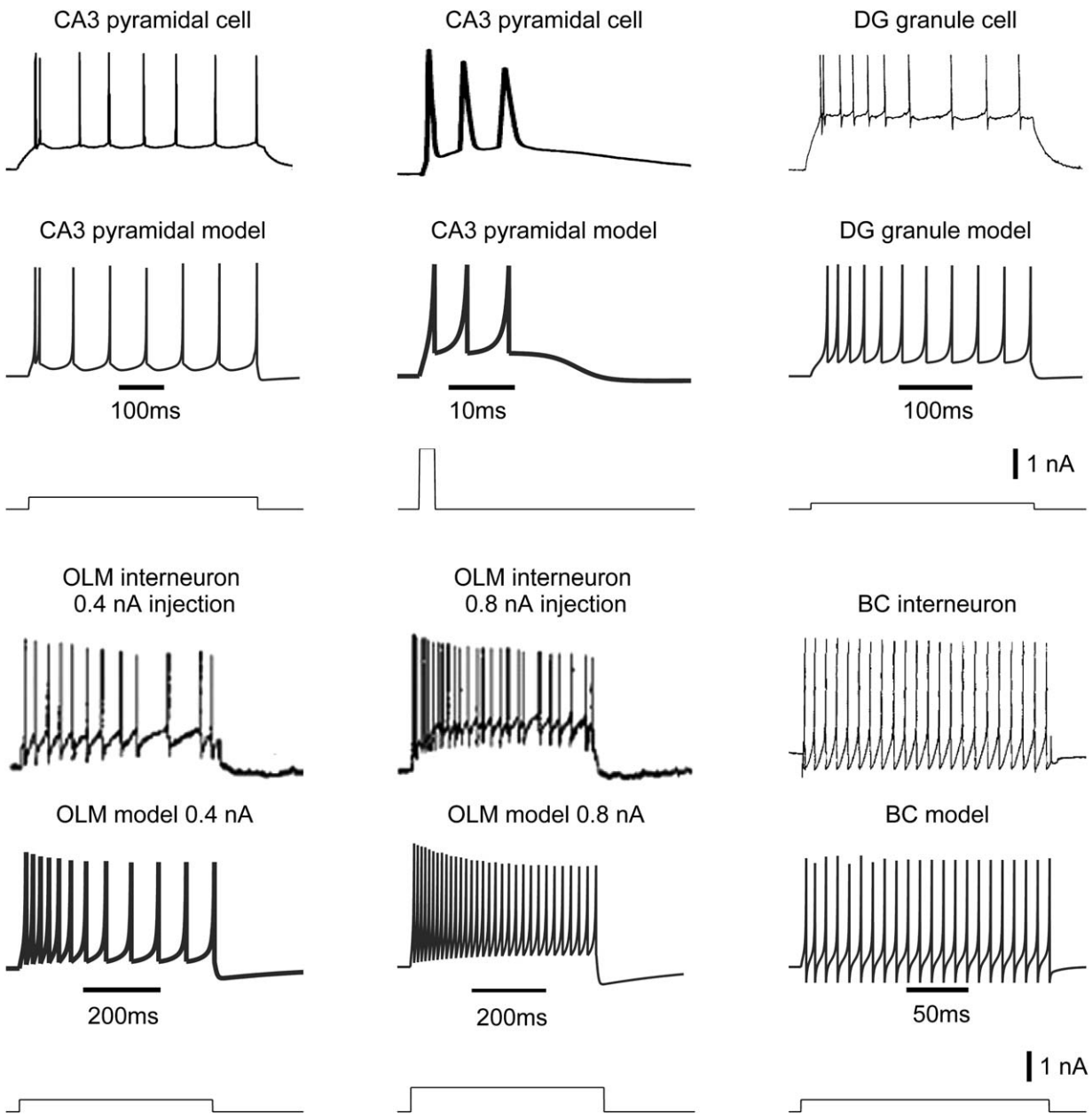

FIGURE 1. ***In vitro*** **current injection recordings of the cell types and their matching model cells. Current injections used in both experimental recordings and model are displayed underneath each pair of recordings and model traces. Sources for the experimental data: CA3 pyramidal cell (Brown and Randall, 2009), DG granule cell (Staley et al., 1992), OLM cell (Ali and Thomson, 1998), and basket cell (Buhl et al., 1996). The parameter values for the model cells are in Table S1 of Supporting Information.**

the other on the longitudinal axis of the hippocampus, and a single neuron in EC can project to about 25% of the longitudinal length of CA3 (Witter, 2010). Projections from DG to CA3 (the indirect pathway) also follow a similar longitudinal organization; however, these projections target a more limited longitudinal extent (Fig. 2A,C; Witter, 2010).

Model cells were distributed in 3D space separated into the three regions, EC, DG, and CA3, with dimensions that approximate the respective dimensions of the rat hippocampus (see Section S3.2 of Supporting Information). Projections from EC to both pyramidal cells and BCs in DG and CA3 followed a lamellar pattern where neurons were most likely to connect to neurons in the center of their longitudinal neighborhood with a decreasing probability toward the periphery. This spatial connectivity was modeled using a Gaussian connection probability function that depended on the longitudinal distance

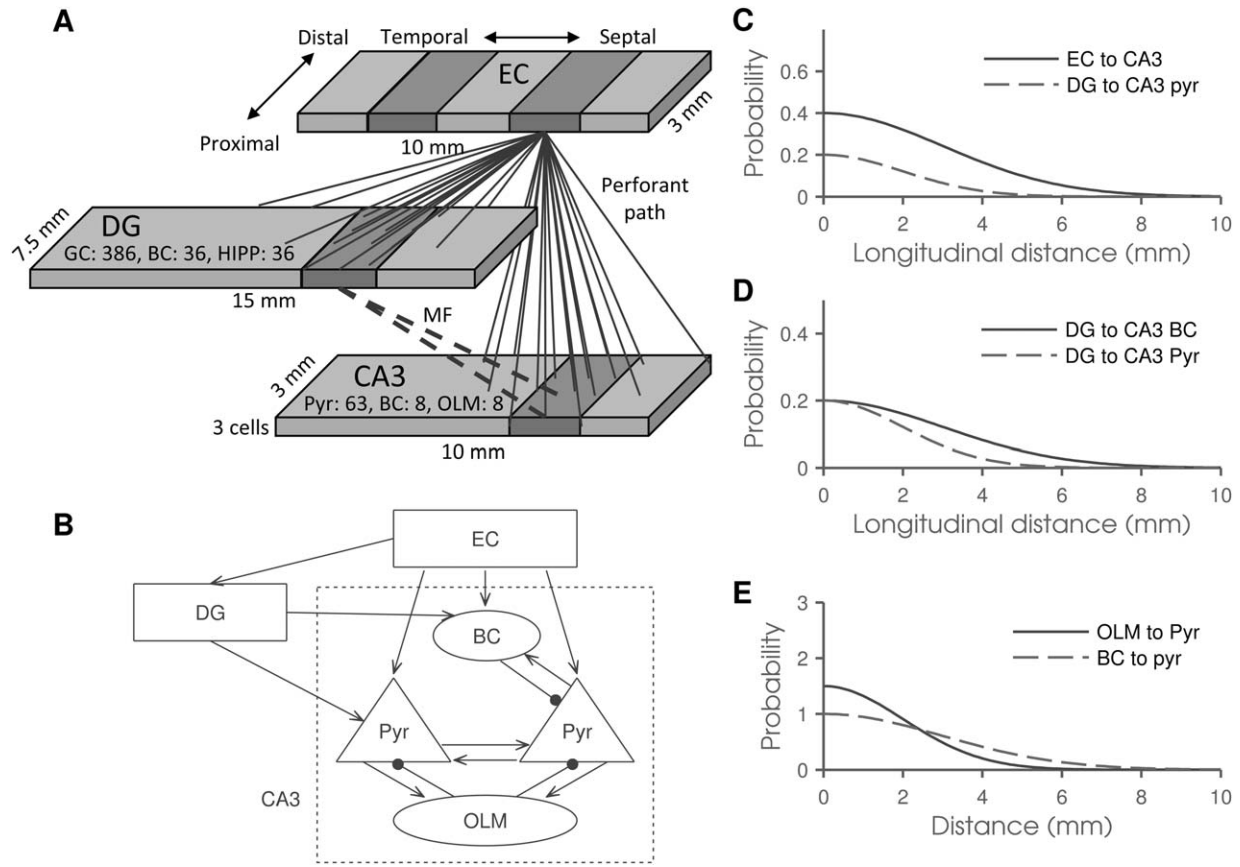

FIGURE 2. Network 3D structure and CA3 local circuitry. (A) Schematic of the network implemented showing the modeled regions EC, CA3, and DG with their dimensions, cell numbers, and lamellar connectivity pattern. Neurons in EC are more likely to send connections to DG and CA3 neurons in their longitudinal vicinity. Similarly, DG granule cells in the same longitudinal neighborhood are likely to project to CA3 neurons in the same lamella. Cells were compacted into three sheets of cells, in the radial dimension, representing stratum-pyramidale in CA3 and the granular layer in DG. (B) Schematic with details of CA3 internal circuitry. Excitatory connections terminate in arrows and inhibitory ones in black filled circles. (C) Gaussian connection probability functions. The longitudinal organization of EC inputs to CA3 is compared to DG inputs. Inputs from DG had a more focused pattern of connectivity (see Table S3 for parameter values). (D) Projections from MF to BCs had a wider longitudinal extent, compared to the ones from MF to CA3 pyramidal cells (pyr). (E) The probability of an interneuron connecting to a pyramidal cell depended on the distance between the two in the longitudinal and transverse planes. Note that probability for the OLM domain exceeded one to ensure that OLM cells made dense connections in their immediate neighborhood.

between the two cells to be connected (Fig. 2C,D). The Gaussian function had a peak probability value of 0.4 and a standard deviation of 3 mm for the perforant path projections to both pyramidal and BCs in CA3 (Fig. 2C). Perforant path projections to DG had similar values as listed in Supporting Information Table S3.

Similarly, MF projections from DG to CA3 followed the same lamellar pattern but with a more limited longitudinal extent by setting the standard deviation of the Gaussian probability function to 2 mm (Fig. 2C). In addition, to preserve the sparseness of the MF connections from DG to CA3, each DG granule cell connected to a maximum of two CA3 pyramidal neurons (Rolls and Kesner, 2006). Projections from DG granule cells to CA3 BCs are more diffuse and out-number projections to CA3 pyramidal neurons by a ratio of 10:1 (Acsady et al., 1998). Accordingly, DG projections to BC followed a Gaussian distribution with a peak probability of 0.2 and standard deviation of 3 mm (Fig. 2D). Recurrent CA3 connections generally reveal no spatial organization (Wittner et al., 2007), and therefore were distributed homogenously with a fixed probability of 0.3.

The dendritic projecting OLM cells are thought to be involved in feedback inhibitory loops (Maccaferri, 2005) and while they have a more limited axonal arborization (Buhl and Whittington, 2007) they make many more synapses compared to BCs (Sik et al., 1995). In contrast, BCs have a more diffuse axonal arborization with the highest connection probability to pyramidal cells in their immediate neighborhood and a decreasing connection probability toward the periphery of their axonal arbors (Sik et al., 1995). Similarly, BCs project to neighboring OLM cells (Bartos et al., 2010). As before, we used a Gaussian function to approximate these spatial

TABLE 1.

Summary of Parameters Used in the CA3 Network Model

	EC input	MF input	Recurrent	Pyr to OLM	Pyr to BC	OLM to pyr	BC to pyr
Spatial connectivity	Diffuse (Witter, 2010)	Focused (Witter, 2010)	Homogenous (Wittner, 2007)	Reciprocal (Maccaferri, 2005)	Homogenous (Wittner, 2006)	Dense, compact (Buhl et al., 2007)	Light, diffuse (Buhl et al., 2007)
AMPA or $GABA_A$ rise/decay time constants (ms)	1.7/10.9 (Tóth, 2010)[a]	0.7/10 (Tóth, 2010)[a]	1.1/5 (Hoskison et al., 2004)	0.27/0.57 (Geiger et al., 1997)	0.27/0.57 (Geiger et al., 1997)	2.8/20.8 (Bartos et al., 2010)[a]	0.21/3.3 (Bartos et al., 2010)[a]
Weight	2	0.2	0.4	3	3	3	3
Short-term plasticity	None	Facilitating (Toth et al., 2000)	Depressing (Hoskison et al., 2004)	Facilitating (Ali and Thomson, 1998)	Depressing (Ali et al., 1998)	None	Depressing (Hefft and Jonas, 2005)
ACh effect	Suppressed (Kremin and Hasselmo, 2007)	Enhanced (Vogt and Regehr, 2001)	Suppressed (Kremin and Hasselmo, 2007)	None	None	None	None
Learning rate	20	0	5	2.5	2.5	2.5	2.5
LTD threshold	0.2	N/A	0.1	0.2	0.2	0.2	0.1
LTP threshold	0.4	N/A	0.2	0.4	0.3	0.7	0.3

[a] We calculated the rise time constant from the reported 20–80% rise time or 10–90% rise time, see Supporting Information Table S3.

probabilities (Fig. 2E). We also assumed that BC projections to both pyramidal cells and to OLM cells shared the same spatial domain. Section S3.2 of Supporting Information has additional details.

In the reverse direction, OLMs receive reciprocal connections from the same pyramidal cells they projected to, in line with their function as local feedback cells (Maccaferri, 2005). On the other hand, principal cells in both DG and CA3 projected homogenously to BCs with a fixed probability of 0.15, consistent with the lack of specific topography reported at these projections (Wittner et al., 2006).

The network was constructed by generating connections randomly between cells while observing the connection probabilities and the spatial patterns of connectivity described above and in Section S3.2 of Supporting Information. For each experiment, we performed 10 random initializations of the network and averaged the results. The spatial connectivity patterns are summarized in Table 1, and parameters for synapses are listed in Supporting Information Tables S3 and S4. Spontaneous firing rates of pyramidal cells in CA3 (Mizuseki et al., 2012) and granule cells in DG (Bower and Buckmaster, 2008) were matched to experimental reports in the full network.

Synaptic Currents

Synaptic currents were modeled using the kinetic models described by Destexhe et al. (1998). The synaptic currents AMPA, NMDA, $GABA_A$, and $GABA_B$ were modeled and their dynamics such as rise and decay time constants and delays were matched to available literature. In particular, CA3 pyramidal cell AMPA currents were fastest for MF inputs from DG and slowest for perforant path inputs from EC, while recurrent CA3 inputs from other pyramidal cells had intermediate values, as summarized in Table 1 (Hoskison et al., 2004; Tóth, 2010). Additionally, inhibitory currents from OLM had slower dynamics compared to those from BC (Table 1; Bartos et al., 2010). Equations implemented are described in detail in Section S4.1 in Supporting Information and parameters used are listed in Tables S3 and S4.

Synaptic weights were assigned in accordance with literature where available (see Tables 1, Supporting Information Tables S3 and S4). The MF synapses were adjusted so that a train of spikes arriving at the synapse could cause a CA3 neuron to fire while a single spike could not (Henze et al., 2002). Recurrent CA3 collaterals were assigned a low initial weight, as an approximation of data showing that action potentials have a transmission probability of 4% at those synapses (Miles and Wong, 1986). Synapses from CA3 pyramidal to interneurons were set at a higher level considering that action potential transmission occurs at a ~60% success rate (Miles, 1990; Gulyás et al., 1993). Connections between granule cells and DG interneurons were adjusted to achieve sparse DG firing (Bower and Buckmaster, 2008). These assigned synaptic weights are listed in Tables 1, Supporting Information Tables S3 and S4. Synapses had initial weights chosen from a uniform

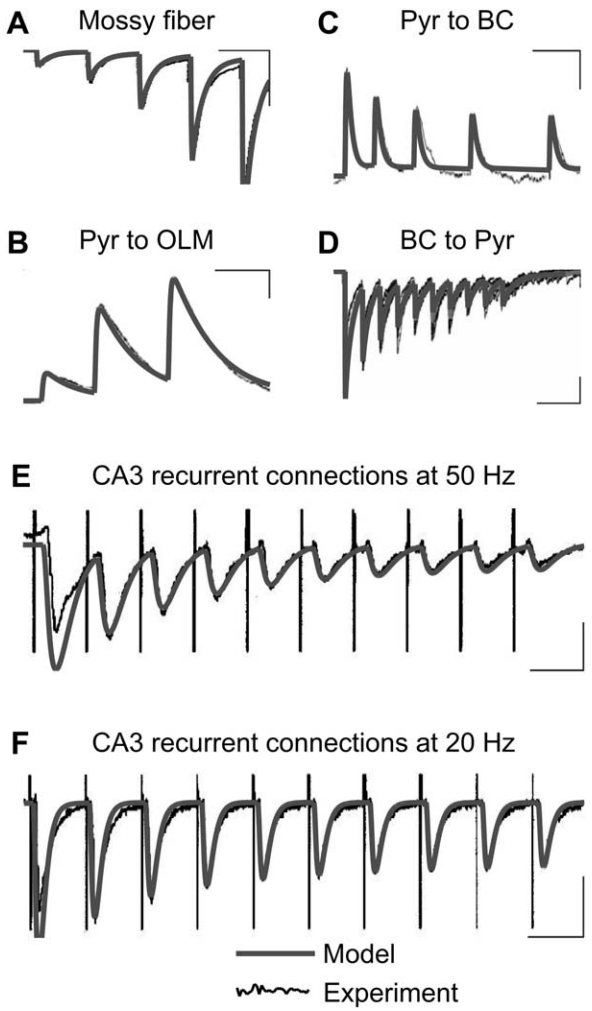

FIGURE 3. Matching short-term plasticity to experimental recordings. Short-term plasticity was modeled using equations proposed by Varela et al. (1997) and parameter values were obtained by matching model to experimental recordings. Note that depending on available data, some panels display the postsynaptic cell membrane potential and others display the synaptic current. Parameter values used to reproduce data are listed in Supporting Information Table S5. (A) Mossy fiber synaptic facilitation (Toth et al., 2000; scale bars: 50 ms, 100 pA). (B) CA3 Pyramidal cell to OLM interneuron (Ali and Thomson, 1998; scale bars: 20 ms, 1 mv). (C) CA3 Pyramidal cell to BC interneuron (Ali et al., 1998; scale bars: 30 ms, 0.5 mv). (D) BC interneuron to CA3 pyramidal cell (Hefft and Jonas, 2005; scale bars: 50 ms, 100 pA). (E and F) Recurrent CA3 connections stimulated at 50 and 20 Hz, respectively (Hoskison et al., 2004). Note that these connections displayed paired pulse facilitation, a phenomenon not included in our synapse model. Therefore, responses to the first stimulus in the train appear larger than the recordings (scale bars: 20 ms, 0.5 mv in E; 50 ms, 0.5 mv in F).

random distribution, with a range from 50 to 100% of the assigned weight value.

Long-Term Synaptic Plasticity

Classical Hebbian associative long-term potentiation (LTP) was shown at the perforant path synapses to DG (Bliss and Lomo, 1973) and to CA3 (Do et al., 2002; McMahon and Barrionuevo, 2002). On the other hand, the characteristics of MF potentiation are controversial (Bliss et al., 2007), and so we only modeled short-term plasticity in the MF connections, as described below.

At GABAergic synapses, many forms of synaptic plasticity exist (for a review, see Maffei, 2011). Woodin et al. (2003) reported that activation of pre- and postsynaptic neurons in the hippocampus lead to LTP if the pre- and postsynaptic spikes were within 20 ms of each other, LTD if within 50 ms, and no change if longer. They also found this plasticity to be dependent on activation of postsynaptic L-type voltage dependent calcium channels (VDCCs).

To reproduce these experimental findings, long-term postsynaptic plasticity was implemented using a learning rule that used the concentration of a postsynaptic calcium pool at each modifiable synapse (Kitajima and Hara, 1997; Shouval et al., 2002; Li et al., 2009; Kim et al., 2013a, 2013b).

At excitatory synapses in our model, calcium entered postsynaptic pools via NMDA receptors, whereas at inhibitory synapses, calcium entered through VDCCs, and in addition, the postsynaptic pool also received Ca^{2+} from internal stores upon $GABA_B$ receptor stimulation (Gaiarsa et al., 2002). Such as scheme has been in other models by our group (Li et al., 2009; Kim et al., 2013a, 2013b). For both types of synapses, the synaptic weight depressed when calcium concentration of the pool was above a lower threshold and increased if the concentration exceeded an upper threshold. Equations and details related to the learning rule are provided in Section S4.2 of Supporting Information.

Short-Term Synaptic Plasticity

In addition to long-term plasticity, model synapses also exhibited short-term synaptic plasticity that used the formulation proposed by Varela et al. (1997). We modeled the pronounced short-term facilitation at MF (Toth et al., 2000) and the frequency-dependent synaptic depression reported at the recurrent CA3 connections (Fig. 3; Hoskison et al., 2004).

In CA1, projections from pyramidal cells display short-term facilitation at synapses contacting OLM cells (Ali and Thomson, 1998), and short-term depression at those contacting BC cells (Ali et al., 1998). In the other direction, inhibitory currents from OLM cells to pyramidal cells show no short-term facilitation or depression (Maccaferri, 2005), while inhibitory currents from BCs to pyramidal cells show depression (Hefft and Jonas, 2005). Equations and parameter values used to model these short-term plasticity patterns are provided in Section 4.2 and Table S5 of Supporting Information, and model traces are compared with available experimental recordings in Figure 3.

Acetylcholine Effects

The neuromodulator acetylcholine activates two main classes of receptors, both of which are present in the hippocampus: muscarinic receptors that are coupled with a G-protein

signaling cascade, and nicotinic receptors that are fast ionic channels. The hippocampus receives widespread volume transmission of cholinergic inputs from the septum-diagonal band complex (Woolf, 1991). To implement the effects of ACh on model neurons and synapses, we used a variable "ACh" to represent the ACh level. The variable ACh had discrete values of 0 (low), 1 (baseline), and 2 (high).

Cholinergic stimulation has differential effects on synaptic transmission of different pathways in the hippocampus (Barry et al., 2012). Synaptic transmission through the perforant pathway projections to CA3 is suppressed by 50%, compared to a suppression by 85% at the recurrent connections in CA3 (Hasselmo et al., 1995; Kremin and Hasselmo, 2007). On the other hand, MF transmission is enhanced by 49% (Vogt and Regehr, 2001).

To model ACh effects on synapses, AMPA synaptic currents were scaled by the value of ACh. A parameter bACh determined the direction and magnitude of ACh effects on a particular synapse. Values of bACh for different synapses were set according to experimental results as summarized in Table 1. The specific equations used to model these are listed in Section S5.2 of Supporting Information.

In addition to the synapse specific effects, cholinergic stimulation enhanced cellular excitability and depolarized the resting membrane potential of principal cells, eliminated AHP, decreased spike frequency adaptation and induced rhythmic burst activity (Misgeld et al., 1989; Bianchi and Wong, 1994). Furthermore, effects on interneurons were subtype dependent (McQuiston and Madison, 1999a, 1999b). Muscarinic stimulation of OLM interneurons depolarized the resting membrane potential, and lowered both spike frequency adaptation and AHP (Lawrence et al., 2006). In contrast, PV-BCs express low levels of nicotinic ACh receptors, and respond to muscarinic receptor activation with a limited resting membrane potential depolarization (Ceadel Rio et al., 2010; Cobb and Lawrence, 2010).

Effects of ACh on neurons were modeled by linearly scaling the neuronal model parameters by the ACh level as shown in Supporting Information Figure S4 and detailed in Section S5.1 of Supporting Information. This setup produced a different set of parameter values for model neurons at low, baseline and high levels of ACh as listed in Supporting Information Table S2. Considering the slow dynamics of ACh effects (onset time constant approximated between 1 and 2 s; Hasselmo and Fehlau, 2001), ACh level was set to a given value at the beginning of each experiment and had no dynamics.

Inputs and Data Analysis

Recordings from the hippocampus reveal a low spontaneous firing rate of 0.50 ± 0.78 Hz in CA3 (Mizuseki et al., 2012) and similar rates in DG (Bower and Buckmaster, 2008). Principal cells in CA3 and DG received random Poisson inputs to generate the spontaneous firing rates reported *in vivo* in the network.

To test the robustness in response to a wide range of input intensities, the network was challenged with 30 trials of increasing levels of input from EC. Each trial had a duration of 500 ms at the beginning of which a number of EC neurons were selected to receive one action potential each. Starting with Trial 1 where one EC neuron was stimulated, one additional neuron received input for each subsequent trial until 30 neurons were stimulated at Trial 30. This input structure was created so that a gradually increasing number of EC neurons fired one action potential at the beginning of the trial. This EC input was transmitted through the perforant pathway to the downstream CA3 and DG regions. For each neuron in CA3, the number of spikes fired during each trial was recorded, and the neuron was considered active if it had a z-score higher than 2.58 ($P < 0.01$, two tails), where $z =$ (firing rate $-$ mean spontaneous firing rate)/SD. For each experiment, we report the ratio of active to inactive neurons in CA3 to follow the dynamics of how rapidly cells are recruited into the pool of active cells, as intensity of input from EC increases.

Simulation Details

The model was developed using the NEURON package and run on a PC with an Intel i7-core processer with an integration time-step of 0.1 ms (Carnevale and Hines, 2009). The recorded spike times were then analyzed using MATLAB (Mathworks).

As mentioned above, cell models had membrane potential values drawn from a random distribution. Additionally, network connectivity, and initial synaptic weights were also drawn from random distributions. Accordingly, for each experiment, 10 simulations with different random initializations of the network were considered. Numbers reported in results are averages $\pm$ SD over data from these 10 different runs.

Model Tuning and Validation

The overall model was developed in stages: the single cell models, the properties of glutamatergic and GABAergic synapses, the intrinsic connections between cells, plasticity in appropriate connections, and, finally, neuromodulator effects. The following approach was used for modeling each of the above: (1) the experimental literature was mined, both to constrain the model and derive criteria to assess whether the model successfully reproduced the particular phenomena being modeled; (2) iterative "tuning" of model parameters was performed until the model's behavior matched experimental observations; and (3) validation of the model, which took two forms. First, the ability of the model to reproduce the experimental data considered in its development. Second, the ability of the model to reproduce a set of experimental observations it was not designed to reproduce. The tuning and validation procedure used are described next.

Model tuning

To further constrain the model and assess its functional capacity, we tuned it to perform pattern separation and pattern completion. The additional tuning required was mainly to adjust connection weights and LTP thresholds (Supporting

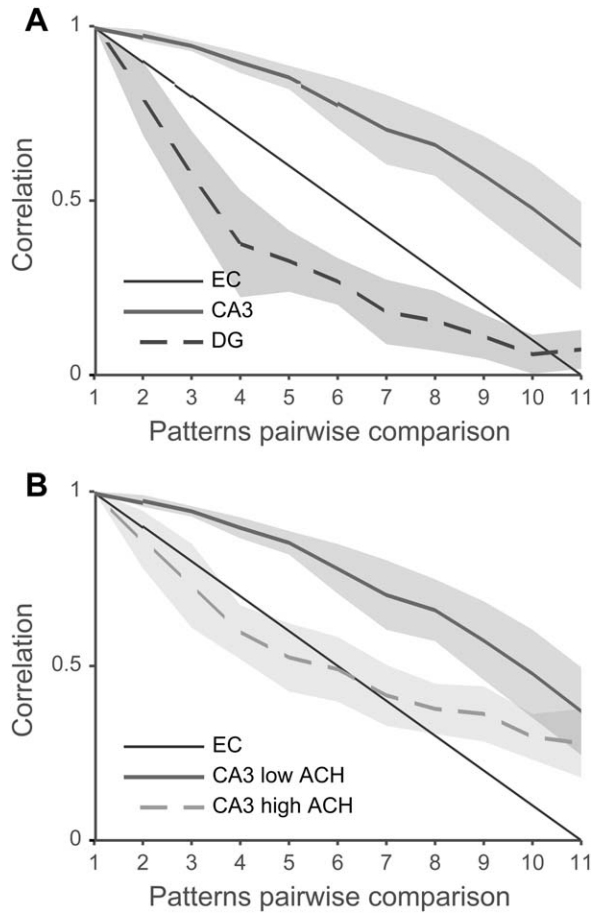

FIGURE 4. Pattern completion and separation in CA3 and DG. The network learned Pattern 1 for five trials under high levels of ACh. Subsequently, long-term plasticity was inactivated to test retrieval in response to inputs Patterns 1–11. Output spikes were recorded at EC, CA3, and DG, and correlation was calculated between the output from Pattern 1 and the output from each of the test patterns. Results were averaged over data from 10 randomly constructed networks and shaded areas indicate standard deviation. (A) Correlation of output patterns produced at EC, CA3 and DG in response to probe Patterns 1–11. The correlation between input Pattern 1 and the probe patterns at EC is shown as a reference point. Correlation values at CA3 pyramidal neurons lie well above the input correlation indicating a tendency toward pattern completion in CA3. Conversely, DG correlation values lie below input correlation levels indicating pattern separation. (B) The effects of low vs. high levels of ACh during retrieval on correlation levels in CA3.

Information Tables S3 and S4), to ensure practical neuron activity levels and synaptic learning rates.

Following Hasselmo et al. (1995), we ran the network through an encoding phase under high levels of ACh (=2). In this encoding phase, an input pattern was constructed to consist of 10 randomly selected EC neurons (Pattern 1), and the network was then presented with this input pattern for five 500 ms trials. For each trial, EC neurons in the pattern received inputs for 250 ms at 12 Hz.

After the encoding phase, we tested for retrieval in response to 10 input patterns that had decreasing amounts of overlap with the encoded Pattern 1. The 10 probe patterns, numbered 2–11, were constructed as follows. Pattern 2 contained nine of the neurons in Pattern 1 and an additional neuron selected randomly. Similarly, Pattern 3 shared eight neurons with Pattern 1 and included two other neurons selected randomly. With this logic, Pattern 11 had no neurons in common with Pattern 1. To test for retrieval, all long-term plasticity was inactivated and we examined the output retrieved in response to probe Patterns 2–11 under the lowered (retrieval) level of ACh (=0).

In each retrieval trial, 1 of the 11 patterns was presented at EC, and the number of spikes each neuron fired during the trial was recorded. Subsequently, to form a trial "output" pattern for each area, the spike counts from all its principal cells were populated into a vector that was normalized to a length of one. The correlation between the outputs of any two trials was then assessed by taking the dot product of the two corresponding output vectors. This correlation measure has a minimum value of 0 indicating that the two output patterns being compared had a nonoverlapping set of neurons firing in each. Conversely, a correlation level maximum value of 1 indicates that the two vectors had the same set of neurons firing at the same rates.

For each area in the model, we calculated pair-wise correlation comparisons between the output from Pattern 1 and the output from each of the patterns from 1 to 11. Figure 4 shows these pair-wise correlation values for EC, CA3 and DG averaged from 10 different randomly constructed model networks. Inputs arrived directly at EC neurons, thus, EC correlation levels reflect the similarity between input patterns. Correlation between CA3 output patterns were above EC correlation (Fig. 4A), indicating that CA3 was engaged in retrieval of stored patterns. For instance, input Pattern 3 had a correlation of 0.8 with input Pattern 1, whereas in CA3, the output from Pattern 3 had a correlation of 0.98 with Pattern 1, indicating that even for dissimilar inputs CA3 retrieved output that are more similar to the learned Pattern 1. Thus, even with changes in the sensory input, CA3 may still retrieve a previously learned memory pattern. On the other hand, DG outputs revealed lower correlation relative to inputs, indicating that DG was predisposed to create distinct neuronal representations (Fig. 4A).

These results are consistent with computational theories of the division of labor between DG and CA3 (Treves and Rolls, 1992; O'Reilly and McClelland, 1994; Hasselmo et al., 1995; McClelland and Goddard, 1996) and recent experimental evidence (Lee and Kesner, 2004; Leutgeb et al., 2007; Bakker et al., 2008; Neunuebel and Knierim, 2014).

Model validation

Cholinergic transmission has been implicated in the modulation of activity in CA3 with high ACh favoring pattern separation and low ACh levels favoring pattern completion (Hasselmo et al., 1995; Rogers and Kesner, 2003; Meeter et al., 2004). Accordingly, to validate the model, we examined the effects of different levels on ACh on the dynamics during retrieval, and compared the results to reports in the literature.

Averaged results from 10 random initializations of the network demonstrated that CA3 outputs in response to probe Patterns 1—11 had significantly lower correlation levels to the encoded Pattern 1 under high levels of ACh compared to low ACh levels (Fig. 4B), while DG correlation levels remained unchanged (not shown). These observations are in agreement with previous models (Hasselmo et al., 1995; Meeter et al., 2004; for review, see Newman et al., 2012) and experimental results (Ikonen et al., 2002; Rogers and Kesner, 2003, 2004).

Limitations

The Izhikevich neuron model formulation focuses on the dynamics around the resting state of the neuron and our modeling efforts aimed at reproducing the current injection responses such as spiking dynamics, adaptation and bursts. Model resting membrane potentials, threshold voltage, and peak action potential were matched to experimental values, but the input resistance was not. As cited, we did match current injection responses and so feel that the firing dynamics were modeled well. The Izhikevich formulation also allows for other currents to be added, further improving single cell characteristics, if required.

Also, we note that synapses from DG granule cells to CA3 parvalbumin-BCs exhibit short-term synaptic facilitation (Szabadics and Soltesz, 2009). However, inputs from MF to other types of interneurons such as Cholecystokinin-BC exhibit short-term depression. Therefore, we assumed that the combined input from DG to both populations of BC cells would then effectively have no short-term dynamics. Accordingly, the MF synapses to BCs in the present model did not have any short-term plasticity.

RESULTS

Our network model included the CA3 and DG regions of the hippocampus, with EC providing inputs to both regions (Fig. 2). The model also incorporated the effects of cholinergic modulation proposed by Hasselmo et al. (1995) and showed similar dynamics discussed next.

Under high levels of ACh, the DG formed distinct representations of input patterns, mainly due to the large numbers of DG granule cells. High ACh levels caused granule cells to fire at a higher rate through a more depolarized membrane potential, lower spike frequency adaptation, and lower AHP. This increased rate, combined with the prominent short-term facilitation at MF synapses, allowed high ACh levels to enhance the flow of information from DG to CA3. Furthermore, the high cholinergic state also suppressed synaptic transmission at the inputs from EC to CA3 and at the recurrent synapses in CA3; thereby decreasing any interference produced by similarity to any previously learned patterns during the encoding of new patterns. Additionally, the abundant connections from DG to CA3 BCs further increased the level of inhibition on CA3 pyramidal cells and reduced the activation of previously encoded memory patterns. In contrast, during the retrieval of stored patterns in the low cholinergic state, granule cells fired at a lower rate reducing their influence over CA3 pyramidal cells considerably. Low levels of ACh also boosted inputs to CA3 cells from EC and from other CA3 neurons. These effects facilitated the retrieval of previously learned patterns as also shown in previous models (Barkai et al., 1994; Hasselmo et al., 1995; Hasselmo and Wyble, 1997).

The control that ACh exerts on the firing rate of granule cells, combined with the profound MF short-term facilitation, allowed ACh to gate the synaptic transmission from DG to CA3 effectively. Although this mechanism has been speculated based on experimental results (Vogt and Regehr, 2001), our model functionally implemented this particular mechanism and incorporated it into the framework established by Hasselmo et al. (1995) and Hasselmo and Wyble (1997).

During the development of the model, runaway excitation was a common phenomenon (Hasselmo et al., 1995). To prevent this spread of excitation we included several candidate mechanisms that were successful at stabilizing excitatory activity in the model without affecting the ability to encode and retrieve patterns as shown in Figure 4. After developing and validating the model (Fig. 3), we used the model in its baseline state (prior to training with Pattern 1), to investigate the specific roles of these intrinsic mechanisms in preventing runaway excitation after turning off plasticity and setting ACh to "medium" level. We devised the following method for this analysis: EC neurons were projected to CA3 at increasing levels of activity, over 30 trials, as follows. Selected EC neurons were stimulated to fire one action potential at the beginning of a given trial. Starting with one neuron stimulated during Trial 1, one additional EC neuron received stimulation for each trial, until thirty distinct neurons were stimulated during Trial 30 (see Fig. 5A). This study resulted in several findings discussed in the following sections. We repeated the analysis using the model after it had learned Pattern 1, and found similar results, as we describe later.

Recurrent Connections Create Seizure-Like Instability

To characterize the unstable dynamics in CA3 created by its recurrent connections, DG was turned off and OLM and BC interneurons were disconnected. Additionally, short-term depression was removed from the recurrent connection synapses, all long-term plasticity was blocked, and ACh was set at the baseline "medium" level. The EC neurons were then projected to CA3 at increasing levels of activity, over 30 trials. A typical EC firing pattern throughout the experiment is shown in Figure 5A. Responses of CA3 neurons were then recorded without (Fig. 5B,D1) and with the recurrent connections in place (Fig. 5C,D2). As expected, CA3 population firing rate increased linearly with increasing inputs from EC, when the recurrent connections were disabled (Fig. 5E). In contrast, the population firing rate showed a sudden nonlinear increase when the recurrent connections were present (Fig. 5E). These

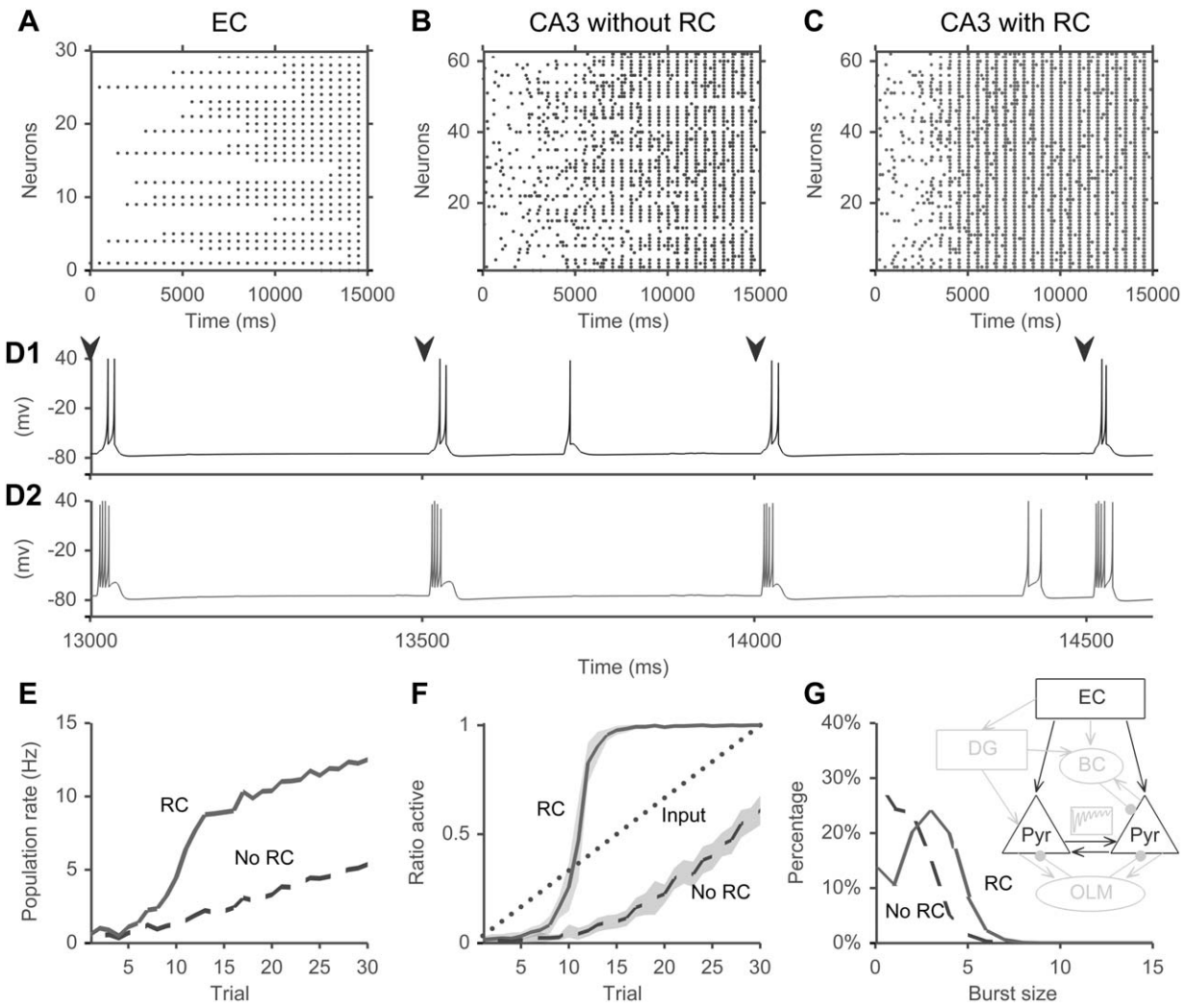

FIGURE 5. The effects of recurrent connections on excitation within CA3. At the beginning of each trial, a stimulus of one action potential was delivered to a number of randomly selected of EC neurons, which projected to CA3. The number of EC neurons stimulated increased with each trial. The DG region and other cell types in CA3 were disconnected, with ACh at baseline levels and no short- or long-term plasticity. (A) Spike raster plot of EC neurons in response to structured inputs for 30 trials from a representative network. Each trial had a 500-ms duration, and for each trial, an increasing number of randomly selected EC neurons received a synaptic stimulus generating one action potential. As can be seen in the plot, only one EC neuron fired on Trial 1 in the first 500 ms, two fired during Trial 2, and so on, ending in 30 neurons firing on Trial 30 in the last 500 ms of the simulation. (B) Spike raster plot of CA3 pyramidal neurons without the recurrent connections in response to the input presented at EC across 30 trials. (C) Spike raster plot of CA3 from a representative network with recurrent connections restored. Spikes are shown for the 30 trials of the experiment. (D) Membrane voltage traces from a representative neuron in the network without recurrent connections (D1) and with recurrent connections (D2). The traces show the membrane voltage response during Trials 22–25, with arrowheads marking the beginning of each trial. (E) Population firing rate histogram for CA3 without recurrent connections (dashed line) and with recurrent connections (solid line). Firing rate was calculated for each trial by averaging trial spike count from all CA3 pyramidal neurons and dividing by trial duration. (F) Ratio of active to inactive neurons in EC (dotted diagonal line), in CA3 without recurrent connections (dashed line) and in CA3 with recurrent connections (solid line). Results are averages of data from 10 networks with different random seeds, and shaded areas represent standard deviation. (G) Changes in distribution of different burst sizes with and without recurrent connections. The distribution was obtained by pooling action potential counts from each neuron in each trial. The data were averaged from running 10 initializations of the network, and presented as a percentage of the total neuron-trial count for each burst size. Inset shows a schematic with model components used in this experiment. Active components are shown in dark lines, while inactive components are shown in light gray lines. RC: recurrent connections.

results are consistent with observations from earlier models (Traub et al., 1987).

While the population firing rate was helpful in detecting instability in the level of excitation, from a computational perspective, it is not the only relevant measure. We are interested in the ability of the model to form patterns of activity in response to inputs. A pattern is formed meaningfully, when only a subset of neurons are active. Toward this end, we quantified

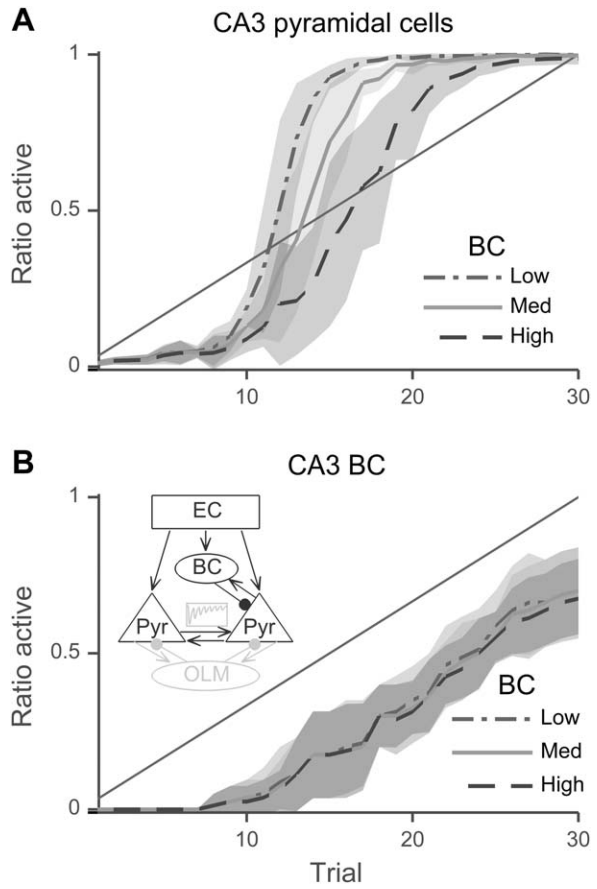

FIGURE 6. Effects of BC interneurons on the stability of CA3 pyramidal cells. The ratio of neurons activated was measured in CA3 in response to increasing EC input over 30 trials. Diagonal line in graphs denotes the rate of input increase at EC. Inhibition by BCs was the only stability mechanism in this experiment, and short-term depression at recurrent connections and inhibition by OLM cells were inactivated. (A) Ratio of active pyramidal neurons for three different levels of BC-to-pyramidal inhibition. Compared to low BC inhibition, medium inhibition shifted the activity ratio curve modestly to the right, without a substantial decrease in its maximum slope. Furthermore, BC inhibition higher than optimized for the pattern separation and completion network did not effectively lower the slope of the curve. (B) The ratio of active BC interneurons showed a linear response with increase in EC inputs, with little difference between the three levels of BC inhibition. Inset shows a schematic with model components used in this experiment. Active components are shown in dark lines, while inactive components are shown in light gray lines.

the ratio of neurons that were "active" for each input trial. A neuron was considered active in a trial if its *z*-score was higher than 2.58 (see Methods). As expected, the activity ratio curve demonstrates the instability caused by recurrent connections (Fig. 5F) and the shape of the curve illustrates the difficulty recurrent connections pose in a model. Low inputs produce little response, and high inputs produce an unstable firing pattern where all cells fire, resulting in a very limited range for forming distinct patterns of activity, i.e., limited capacity to handle variations in input level. Furthermore, the addition of recurrent connections changed the frequency at which bursts of different sizes occurred and caused a peak where bursts of four action potentials were more likely to occur (Fig. 5G).

BCs Fail to Control Instability

As a first step to investigate the control of neuronal excitability in the CA3 network, we activated the fast spiking BCs in CA3, i.e., examined the behavior of the recurrent CA3 network with only BCs added. Considering the importance of BC firing rates at different levels of input, in addition to matching current injection behavior of BCs, we also matched the input-firing frequency curve for one of the BC interneuron reported by Buhl et al. (1996; Supporting Information Fig. S2). The reader is also reminded that connections in both directions from BC to pyramidal and vice versa exhibited short-term synaptic depression (Ali et al., 1998; Hefft and Jonas, 2005). Therefore, in this experiment, OLMs remained disconnected, short-term depression and long-term plasticity were blocked, and ACh was at the baseline "medium" level. The network was tested with three levels of BC-to-pyramidal cells weights; low, medium, and high, with the weight values 0.1, 3, and 6, respectively.

Contrary to expectations, inhibition by BCs was unable to prevent instability in the CA3 network (Fig. 6A), and merely shifted the curve of the ratio of active neurons to the right with minimal effect on the profile of exponential increase. Even for high levels of BC inhibition, the minimal decrease in slope was not sufficient to stabilize the network during encoding and retrieval. We also determined the ratio of active BCs using *z*-scores (Fig. 6B). Interestingly, despite receiving direct inputs from pyramidal cells that increased exponentially with number of trials, BCs continued to respond linearly with trials due to short-term depression at the pyramidal-to-BC synapses.

OLM Interneurons and Short-Term Depression in Recurrent Connections Can Control Instability

We then asked whether OLM cells by themselves could provide the inhibition characteristics required to contain the instability in the CA3 network. To isolate the effects of OLM cells, we kept the same conditions as in the previous section except for disconnecting BCs and connecting OLM cells instead. As noted in methods, OLM cells received input from pyramidal cell with synapses exhibiting short-term facilitation (Ali and Thomson, 1998). This CA3 network was tested with low, medium and high levels of OLM inhibition (OLM to pyramidal weights 0.1, 3, and 6, respectively). Despite their slow dynamics, OLM cells were surprisingly effective in controlling the instability (Fig. 7A). Higher levels of OLM inhibition moved the curve for the ratio of active pyramidal cells closer to linearity and decreased its slope below the curve for inputs increase (Fig. 7A). In addition, recruitment of OLM neurons into the "active" pool showed a sudden nonlinear jump even for high levels of OLM inhibition during which pyramidal cells showed a near linear increase (Fig. 7A,B). This increased recruitment permitted OLM cells to contain instability in CA3 responses effectively.

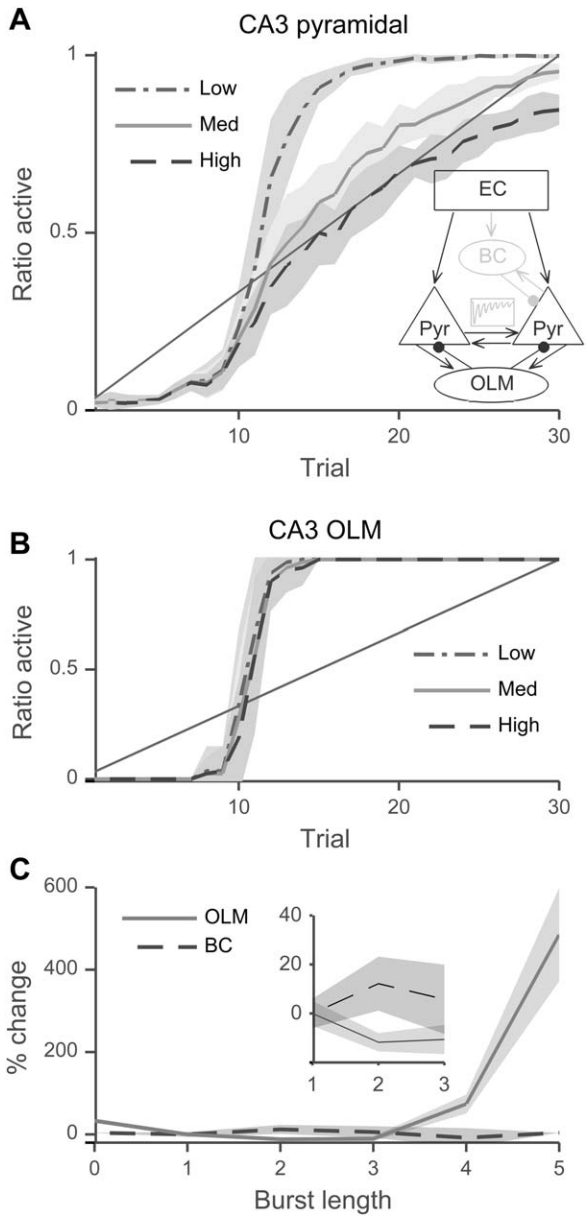

FIGURE 7. OLM interneurons stabilize CA3 and control burst size. The network was tested over 30 trials with increasing amounts of EC inputs, denoted by the diagonal line. Short-term depression at recurrent connections was blocked and BC interneurons inactivated. (A) The ratio of active CA3 pyramidal neurons at three different levels of OLM inhibition. (B) The ratio of active OLM interneurons for low, med, and high OLM-to-pyramidal inhibition showed a nonlinear OLM response. The response of OLM cells continued to be nonlinear even with high inhibition where CA3 pyramidal cells show a controlled near linear response. (C) The percentage change in the occurrence of different burst sizes when inhibition level is lowered from high to low, for BC inhibition (dashed line) and OLM inhibition (solid line).

To allow a qualitative comparison with results from optogentic silencing of BC and OLM cells *in vivo* (Royer et al., 2012), we calculated the change in the occurrence of bursts of different sizes when either OLM or BC inhibition was lowered from high to low. Consistent with experimental findings (Royer et al., 2012), lowering OLM inhibition significantly increased the occurrence of bursts of five or more action potentials, whereas lowering BC inhibition modestly increased the frequency of bursts of two action potentials (Fig. 7C).

Next, we tested the effects of short-term depression in the recurrent CA3 connections as the sole stabilizing mechanism. For this, we disconnected BC and OLM cells and tested low, medium and high levels of short-term depression (d1 = 0.9, 0.7, 0.5, d2 = 0.98, 0.92, 0.86, respectively; equations in Section S4.2 in Supporting Information). Note that the short-term depression parameters for medium levels were obtained by matching experimental recordings of recurrent CA3 connections (Fig. 3, Hoskison et al., 2004). Similar to the effects of OLM inhibition, simulations revealed that higher levels of short-term depression also decreased the rate of CA3 pyramidal cell recruitment below the rate of input increase (Fig. 8A). The

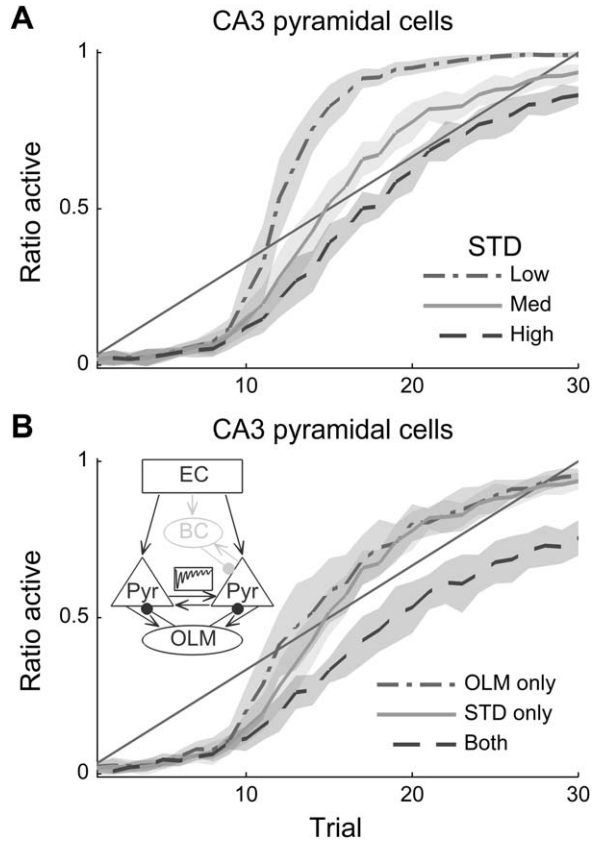

FIGURE 8. Recurrent connections short-term depression stabilizes CA3 activity. (A) The effect of short-term depression (three levels) at the recurrent connections on the ratio of active cells in CA3 with increasing input from EC. Both OLM and BC were inactivated. Baseline or "med" values were obtained by matching experimental data (Hoskison et al., 2004; d1: 0.7, d2: 0.92) and then low (d1: 0.5, d2: 0.86) and high (d1: 0.9, d2: 0.98) levels were created symmetrically around the baseline values. Higher levels of short-term depression stabilized CA3 responses and the curve of ratio of active cells became closer to linear and dropped below the curve for the inputs. (STD: short-term depression). (B) The effects of experimentally matched levels of OLM inhibition or of short-term depression alone compared to the case when both mechanisms were simultaneously active.

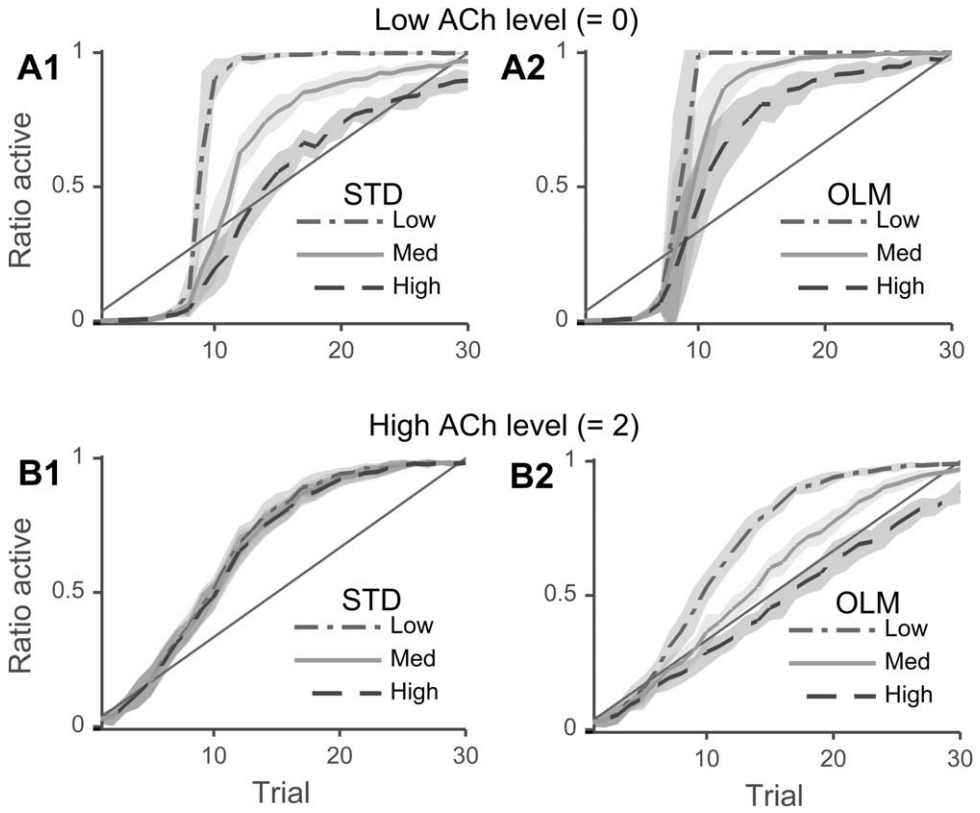

FIGURE 9. The encoding circuit is stabilized by OLM inhibition and the retrieval circuit is stabilized by short-term depression at the recurrent CA3 connections. Ratio of active CA3 pyramidal cells was evaluated for low and high ACh levels with either short-term depression or OLM inhibition activated at three levels. (A) The effects of three different levels of short-term depression at the CA3 recurrent connections (A1), and of OLM inhibition (A2) under low levels of ACh. (B) With high ACh, short-term depression at the CA3 recurrent connections had little effect (B1) while OLM inhibition was critical to the stability of the network (B2).

magnitude of this effect was sufficient to increase the input range at which the model can form patterns to support encoding and retrieval.

Finally, activating either OLM inhibition or short-term depression alone at their "baseline" levels, which were matched to experimental recordings, was not sufficient to reduce the rate of activity increase in CA3 below the rate of input increase at EC, and rather, higher than experimentally reported levels were necessary. Accordingly, a test with both mechanisms active at the experimentally reported "baseline" levels revealed that the presence of both mechanisms reduces the rate of recruitment of pyramidal cells effectively (Fig. 8B).

High and Low Cholinergic States Require Different Stabilizing Mechanisms

The findings so far indicated that while BCs were incapable of stabilizing the CA3 network at baseline (medium) levels of cholinergic transmission, both inhibition by OLM cells and short-term depression at the recurrent connections did effectively control the instability. Our interest however extends to stabilizing the network in both low and high cholinergic states, where network instability might be more likely. Therefore, we next investigated the role of OLM inhibition and short-term depression in the full network, including DG, with all synapses and mechanisms active.

Recruitment of CA3 pyramidal cells was accordingly evaluated at low and high ACh levels, with either OLM inhibition or recurrent connections short-term depression active. Model runs revealed that for the low ACh case, short-term depression at the recurrent connections was the critical mechanism to maintain stability (Fig. 9A1) and the effect of OLM cells was no longer sufficient (Fig. 9A2). In contrast, for the high ACh case, short-term depression at the recurrent CA3 connections was by itself ineffective (Fig. 9B1), and OLM cells were the necessary mechanism to maintain stability (Fig. 9B2).

To further investigate these results, we looked at the distribution of burst sizes in CA3 and DG without the stabilizing effects of OLM inhibition and short-term depression (Fig. 10A,B). Interestingly, both low ACh and high ACh caused enhanced bursting in CA3, though with different patterns and different mechanisms, as follows. High ACh levels significantly enhanced MF transmission causing large currents to arrive at CA3 pyramidal cells. This pattern of excitation generated burst sizes that were distributed evenly but also included very long bursts of 20 and 30 action potentials. It is noteworthy that applying a similar

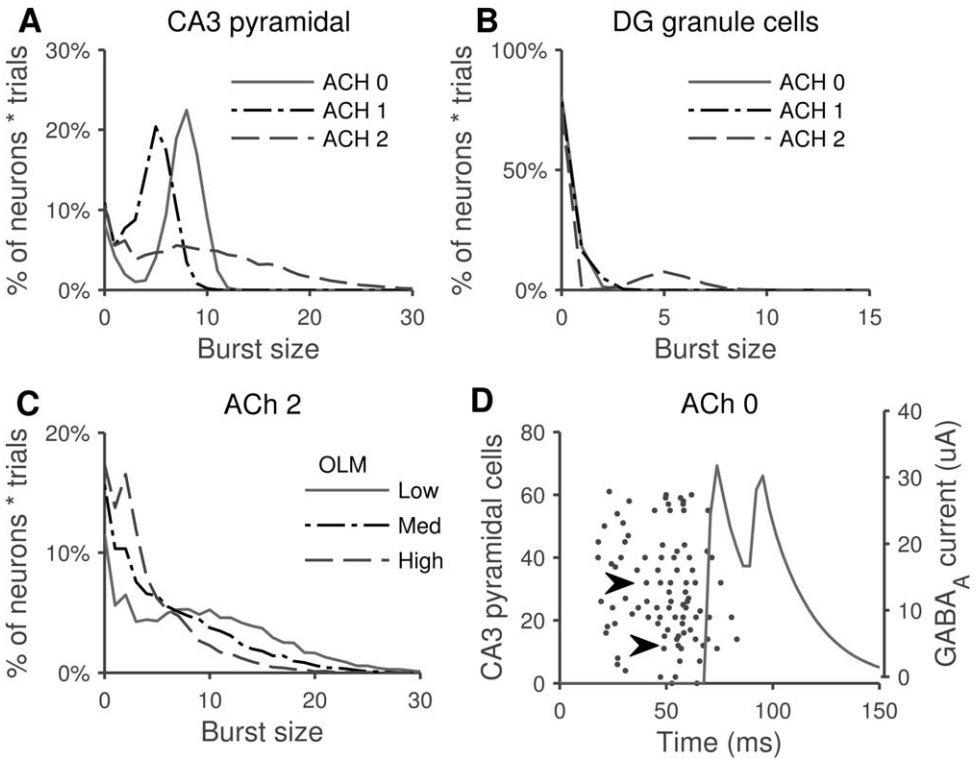

FIGURE 10. Distinct patterns of excitation during encoding and retrieval levels of ACh. Both CA3 and DG networks received increasing inputs from EC without the stabilizing effects of short-term depression or inhibition from CA3 interneurons. The occurrence of bursts of different sizes was calculated across neurons and trials, and is presented as a percentage of all neurons and trials for each burst size. The distribution of burst sizes was considered for low, med, and high levels of ACh. (A) The occurrence of different burst lengths in CA3 under low, med, and high levels of ACh. Low levels of ACh shifted the peak in burst sizes toward longer bursts (peak shifted from five to eight action potentials). Whereas high levels of ACh leads to more distributed burst sizes with a long tail including extended bursts (>20 action potentials). (B) Same analysis as in (A) applied to DG granule cells revealed that these very long bursts were not simply transmitted from DG. High levels of cholinergic transmission in DG caused an increase in the frequency of short bursts in a limited number of granule cells. (C) OLM interneurons were activated in the encoding network (ACh = 2) and the distribution of burst sizes was considered at three different levels of OLM inhibition. Higher levels of OLM inhibition reduced the occurrence of extended bursts. (D) Excitation spread in CA3 network preceded OLM inhibitory current during low ACh levels. One trial is depicted with 20 EC neurons receiving one action potential at time 0. A spike raster plot of CA3 pyramidal cells is shown overlaid with an example of OLM inhibitory current as measured from the soma of a pyramidal cell. Not all pyramidal cells fired in response to the EC stimulus. A few neurons started firing late (Arrows), indicating a di-synaptic source of input from other pyramidal cells. OLM inhibition did not arrive in time to prevent the secondary spread of excitation to these neurons.

analysis as above to DG cells revealed that in response to high ACh, a limited number granule cells fired bursts of five to six action potentials, and consistent with the reported sparse activity in DG (Bower and Buckmaster, 2008), most granule cells were silent (fired 0 action potentials, Fig. 10B). Thus, these very long CA3 bursts were not merely transmitted from the upstream DG region, but rather were likely a product of the large excitatory currents arriving from MF synapses, combined with the ACh effects on CA3 pyramidal cells including membrane depolarization, reduced frequency adaptation, and reduced AHP.

The recurrent CA3 connections contributed but were not the main cause of runaway activity in CA3 during high ACh levels, and as expected, adding short-term depression to these connections did not correct the instability. In contrast, OLM inhibition mainly affected longer bursts of action potentials (Fig. 7C), making it suitable to control these very long bursts. The effects of three different levels of OLM inhibition on the distribution of burst sizes revealed an effective reduction in the occurrence of bursts with more than seven action potentials (Fig. 10C).

On the other hand, compared to baseline levels, low ACh levels shifted the CA3 firing to higher burst sizes. The pattern of enhanced excitation was similar to that generated by the recurrent connections (Fig. 5G), though larger in magnitude, due to the enhanced transmission at recurrent connections induced by low ACh.

The increase in average burst size caused by the enhanced recurrent connections was moderated by short-term depression at these synapses returning the network into a stable state (Fig. 9A1), whereas in the case of OLM interneurons, their slower dynamics resulted in their inhibitory currents arriving after many CA3 pyramidal neurons had discharged bursts of action

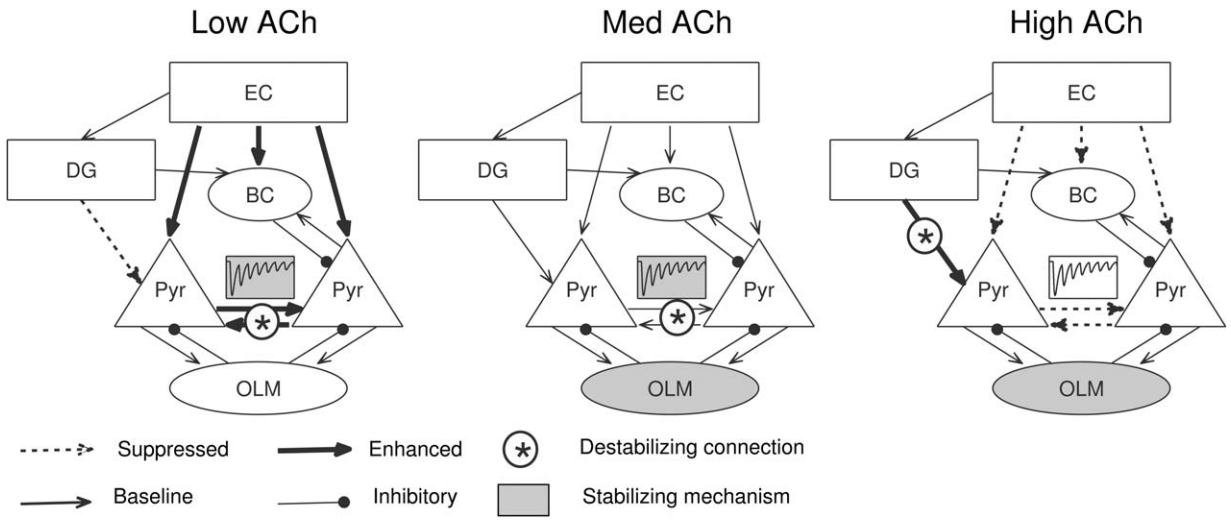

FIGURE 11. Summary of stabilizing mechanisms in low, med and high cholinergic states. Connections are suppressed (dotted arrows) or enhanced (thick arrows) from baseline (normal arrows) by ACh levels. Connections promoting runaway excitation (indicated by *) were the recurrent CA3 connections in low and med ACh states, and MF in high ACh states. On the other hand, mechanisms maintaining network stability (indicated by gray shaded area) were short-term depression in low and med ACh states, and OLM in med and high ACh states.

potentials (Fig. 10D). This revealed a critical result where the ability of OLM cells to contain the instability created by the CA3 recurrent connections depended on the strength of the synaptic transmission at the recurrents. Lower ACh reduced the cholinergic suppression of the recurrent connections and caused excitatory activity to spread rapidly between pyramidal cells well before OLM inhibition arrived (Fig. 10D), whereas at baseline ACh levels, OLM cells were able to fire in time to prevent pyramidal cells from exciting themselves into a runaway state.

We also considered whether the "trained" network (with Pattern 1 encoded) might behave differently. To check this, we compared the stability profile of the trained network to the naïve network. In response to increasing inputs from EC the trained network had a slightly faster activation of CA3 pyramidal cells, but was otherwise identical in behavior (data not shown).

Taken together, these findings suggested that low ACh levels enhance CA3 recurrent connections leading to more sustained bursting in pyramidal cells, and short-term depression at these recurrent connections moderates this excitatory activity, whereas high ACh levels result in very long burst sizes that are optimally controlled by OLM inhibition (Fig. 11).

DISCUSSION

We developed a biophysical model of the hippocampal DG and CA3 regions by matching biological data including single cell behavior, synaptic dynamics, connectivity patterns, and short- and long-term synaptic plasticity. Furthermore, the model was constrained to reproduce the experimentally reported roles of CA3 and DG in pattern completion and separation, respectively. The recurrent connections in CA3 promote runaway excitation, and our results suggested that OLM inhibition and short-term depression at the recurrent connections were effective in preventing this instability, while BC inhibition by itself was not. In addition, our model extended the previously established distinctions between the low and the high cholinergic circuits (Hasselmo et al., 1995) by demonstrating different destabilizing and stabilizing mechanisms in these circuits (Fig. 11). An implication of these findings is that different forms of seizure activity could develop in each circuit through unique mechanisms.

Biologically Constrained Model of Pattern Completion and Separation

Pattern separation and completion in the hippocampus is one of the most prominent computational theories that has been modeled extensively (Treves and Rolls, 1992; O'Reilly and McClelland, 1994; Hasselmo et al., 1995, 2002; Hasselmo and Wyble, 1997; Meeter et al., 2004; Kunec et al., 2005; Cutsuridis et al., 2010; Nolan et al., 2010). The role of cholinergic modulation in these processes has also been modeled using firing-rate neuron models (Hasselmo et al., 1995; Hasselmo and Wyble, 1997) and spiking neuron models (Barkai et al., 1994; Meeter et al., 2004). Hasselmo et al. (1995) considered the explosive growth of excitation in CA3, and revealed that cholinergic modulation itself along with local feedback inhibition aided in stabilizing the network.

Our network model extended previous work by adding components matched to neurophysiological data including two types of interneurons and short-term synaptic plasticity. The

addition of these mechanisms allowed for a more detailed analysis of their role in stabilizing excitatory activity in CA3 during low and high cholinergic states of the network.

In particular, short-term synaptic plasticity influenced the behavior of the model considerably. Based on *in vitro* studies, Vogt and Regehr (2001) suspected that due to the pronounced short-term synaptic facilitation at the MF synapses, cholinergic modulation can indirectly control MF synaptic transmission by modulating the firing rate of DG granule cells. Our model included these dynamics and showed an intact ability to encode and retrieve patterns of activity as regulated by cholinergic modulation (Fig. 4). Furthermore, short-term plasticity in the local connections between pyramidal cells and interneurons shaped the role of interneurons in stabilizing the CA3 network, and short-term depression in the connections between pyramidal cells themselves acted as a robust stability mechanism.

Depressing Synapses Limit Efficacy of BC Interneurons

Considering their rapid dynamics and fast inhibition, BC interneurons appeared well positioned to stabilize the network. However, our findings indicated that BC inhibition in a network of EC and CA3 merely shifted the CA3 input-output curve linearly and could not limit the unstable exponential growth in the recruitment of CA3 pyramidal cells (Fig. 6). These results are consistent with recent recordings from CA3 by Beyeler et al. (2013) that revealed a very limited role for perisomatic inhibitory currents in moderating the recruitment of hippocampal pyramidal neurons. In addition, a different study showed that an increase in parvalbumin-BC inhibitory drive was insufficient to reduce the generation of epileptic discharges in a mouse model of epilepsy (Wyeth et al., 2010).

In our model, this inability of BC cells to control excitation was due to two factors. First, both BC-to-pyramidal (Hefft and Jonas, 2005) and pyramidal-to-BC connections (Ali et al., 1998) displayed short-term synaptic depression. Such dynamics render BC inhibition less relevant at higher firing rates during long bursts of action potentials that occur at the onset of instability. Second, compared to OLM cells, BCs receive less connections from pyramidal cells (Buhl and Whittington, 2007) and also provide fewer connections to pyramidal cells (Sik et al., 1995). The model suggests that these dynamics could explain the reported biological findings (Wyeth et al., 2010; Beyeler et al., 2013).

While our results showed that BCs did not have a significant role in stabilizing the CA3 network, preliminary results from a separate study indicated that they have a prominent role in selecting neurons in a hippocampal ensemble (unpublished data). Further studies are needed to clarify their role in the network.

Nonlinear Mechanisms Play a Critical Role in Stabilization

Activity in CA3 when using only BCs suggested the need for a nonlinear mechanism where suppression of excitation remains modest during low activity levels but increases steeply as activity level increases. While depressing synapses at the recurrent collaterals seemed ideally suited for this task (Sussillo et al., 2007), OLM interneurons were not obvious candidates. Although they provide nonlinear inhibition due to their facilitating inputs, OLM cells exhibit slow membrane dynamics and slow inhibitory currents, project to dendrites, and receive limited direct input from sources other than pyramidal cells (Maccaferri, 2005). However, the model showed that they were effective in limiting the spread of activity at baseline levels of synaptic transmission in recurrent connections.

More specifically, the ability of OLM inhibition to maintain stability of the network was dependent on the level of ACh. At low ACh levels, OLM inhibition failed to stabilize the network mainly due to the rapid spread of excitation through the recurrent connections. Due to the slow dynamics of OLM cells, their inhibitory current arrived at pyramidal cells after excitation has already spread through the network (Fig. 10D). In contrast, at baseline ACh levels, the recurrent connections were relatively suppressed and excitation spread at a slower rate. Therefore, at baseline ACh levels, OLM inhibition arrived in time to prevent the spread of excitation between cells and consequently maintained the stability of the network. Finally, at high ACh levels, the recurrent connections were highly suppressed and were not relevant to network instability. Strong inputs arrived through MF from DG granule cells leading to extended bursts in CA3, and OLM inhibition was well positioned to reduce these bursts and prevent runaway excitation.

Two Distinct Circuits in the Hippocampus

While the presence of two circuits for encoding and retrieval in the hippocampus is well-established (Treves and Rolls, 1992; O'Reilly and McClelland, 1994; Hasselmo et al., 1995), our results extend this perspective. The existence of different dynamics and stability mechanisms revealed a more pronounced distinction between the two circuits (Fig. 11). While both circuits utilize the same physical implementation, the roles of the different components change significantly. In addition to the differences in stability mechanisms reported here, a different study using our model suggested a parallel distinction in oscillatory mechanisms between the two circuits (unpublished data).

These findings suggested that failure of different mechanisms might be implicated in hyperexcitability or seizure-like behavior in the hippocampus during different levels of cholinergic transmission. Considering that levels of ACh are primarily increased with novelty and active exploration (Barry et al., 2012), our model predicts that certain types of seizures are induced by novelty and other types may be facilitated by familiarity. Indeed, rats receiving Domoic acid (an excitatory neurotoxin) during development go on to develop a "novelty-induced seizure-like syndrome" (Doucette et al., 2004; Perry et al., 2009). In these studies, rats developed stereotypical chewing, clonus, and other seizure-like behaviors when placed in a novel Morris water maze. Reports related to a possible familiarity-induced

syndrome have numerous references to the "déjà vu" phenomenon (an intense feeling of familiarity that precedes seizures in humans). However, the relationship between this phenomenon and the actual seizure-behavior remains poorly understood (Martin et al., 2012), which limits any conclusions about the direction of causality. Nonetheless, our model further predicts that the novelty-induced seizures would be a reflection of dysfunction of inhibitory interneurons, while the familiarity-induced counterpart could be due to pathology of excessive excitatory transmission at the recurrent collaterals.

CONCLUSIONS

Findings from our computational model shed light on how intrinsic hippocampal mechanisms might stabilize activity in CA3 during pattern completion and separation phases. Specifically, nonlinear mechanisms such as depressing synapses at recurrent CA3 collaterals or inhibition by OLM interneurons were suited to prevent runaway excitation whereas inhibition by BC interneurons was insufficient. Pattern encoding and pattern retrieval occur through distinct circuits in the hippocampus with different destabilizing and stabilizing mechanisms. These results raise the possibility that different clinical interventions may be required to prevent seizure behavior during distinct modulatory states of the hippocampal network.

REFERENCES

Abbott LF, Nelson SB. 2000. Synaptic plasticity: Taming the beast. Nat Neurosci 3:1178–1183.

Acsady L, Kamondi A, Sik A, Freund T, Buzsaki G. 1998. GABAergic cells are the major postsynaptic targets of mossy fibers in the rat hippocampus. J Neurosci 18:3386–3403.

Ali AB, Thomson AM. 1998. Facilitating pyramid to horizontal oriens-alveus interneurone inputs: Dual intracellular recordings in slices of rat hippocampus. J Physiol 507:185–199.

Ali AB, Deuchars J, Pawelzik H, Thomson AM. 1998. CA1 pyramidal to basket and bistratified cell EPSPs: Dual intracellular recordings in rat hippocampal slices. J Physiol 507:201–217.

Bakker A, Kirwan CB, Miller M, Stark CEL. 2008. Pattern separation in the human hippocampal CA3 and dentate gyrus. Science 319:1640–1642.

Barkai E, Bergman RE, Horwitz G, Hasselmo ME. 1994. Modulation of associative memory function in a biophysical simulation of rat piriform cortex. J Neurophysiol 72:659–677.

Barry C, Heys JG, Hasselmo ME. 2012. Possible role of acetylcholine in regulating spatial novelty effects on theta rhythm and grid cells. Front Neural Circuits 6:5.

Bartos M, Sauer J-F, Vida I, Kulik Á. 2010. Fast and slow GABAergic transmission in hippocampal circuits. In: Cutsuridis V, Graham B, Cobb S, Vida I, editors. Hippocampal Microcircuits. New York: Springer. pp 129–161.

Baude A, Bleasdale C, Dalezios Y, Somogyi P, Klausberger T. 2007. Immunoreactivity for the GABAA receptor α1 subunit, somatostatin and connexin36 distinguishes axoaxonic, basket, and bistratified interneurons of the rat hippocampus. Cereb Cortex 17:2094–2107.

Beyeler A, Retailleau A, Molter C, Mehidi A, Szabadics J, Leinekugel X. 2013. Recruitment of perisomatic inhibition during spontaneous hippocampal activity in vitro. PloS One 8:e66509.

Bianchi R, Wong RK. 1994. Carbachol-induced synchronized rhythmic bursts in CA3 neurons of guinea pig hippocampus in vitro. J Neurophysiol 72:131–138.

Bliss TV, Lomo T. 1973. Long-lasting potentiation of synaptic transmission in the dentate area of the anaesthetized rabbit following stimulation of the perforant path. J Physiol 232:331–356.

Bliss T, Collingridge G, Morris R. 2007. Synaptic plasticity in the hippocampus. In: Andersen P, Morris RGM, Amaral DG, Bliss TVP, O'Keefe J, editors. The Hippocampus Book. New York: Oxford University Press. pp 133–242.

Bower MR, Buckmaster PS. 2008. Changes in granule cell firing rates precede locally recorded spontaneous seizures by minutes in an animal model of temporal lobe epilepsy. J Neurophysiol 99:2431–2442.

Brown JT, Randall AD. 2009. Activity-dependent depression of the spike after-depolarization generates long-lasting intrinsic plasticity in hippocampal CA3 pyramidal neurons. J Physiol 587:1265–1281.

Buhl E, Whittington M. 2007. Local circuits. In: Andersen P, Morris RGM, Amaral DG, Bliss TVP, O'Keefe J, editors. The Hippocampus Book. New York: Oxford University Press. pp 297–320.

Buhl EH, Szilágyi T, Halasy K, Somogyi P. 1996. Physiological properties of anatomically identified basket and bistratified cells in the CA1 area of the rat hippocampus in vitro. Hippocampus 6:294–305.

Carnevale NT, Hines ML. 2009. The NEURON Book. UK: Cambridge University Press.

Cea-del Rio CA, Lawrence JJ, Tricoire L, Erdelyi F, Szabo G, McBain CJ. 2010. M3 muscarinic acetylcholine receptor expression confers differential cholinergic modulation to neurochemically distinct hippocampal basket cell subtypes. J Neurosci 30:6011–6024.

Cobb S, Lawrence JJ. 2010. Neuromodulation of hippocampal cells and circuits. In: Cutsuridis V, Graham B, Cobb S, Vida I, editors. Hippocampal Microcircuits. New York: Springer. pp 187–246.

Cossart R, Bernard C, Ben-Ari Y. 2005. Multiple facets of GABAergic neurons and synapses: Multiple fates of GABA signalling in epilepsies. Trends Neurosci 28:108–115.

Cutsuridis V, Cobb S, Graham BP. 2010. Encoding and retrieval in a model of the hippocampal CA1 microcircuit. Hippocampus 20: 423–446.

Destexhe A, Mainen ZF, Sejnowski TJ. 1998. Kinetic models of synaptic transmission. Methods Neuronal Model 2:1–26.

Do VH, Martinez CO, Martinez JL, Derrick BE. 2002. Long-term potentiation in direct perforant path projections to the hippocampal CA3 region in vivo. J Neurophysiol 87:669–678.

Doucette TA, Bernard PB, Husum H, Perry MA, Ryan CL, Tasker RA. 2004. Low doses of domoic acid during postnatal development produce permanent changes in rat behaviour and hippocampal morphology. Neurotox Res 6:555–563.

Gaiarsa J-L, Caillard O, Ben-Ari Y. 2002. Long-term plasticity at GABAergic and glycinergic synapses: Mechanisms and functional significance. Trends Neurosci 25:564–570.

Geiger JR, Lübke J, Roth A, Frotscher M, Jonas P. 1997. Submillisecond AMPA receptor-mediated signaling at a principal neuron-interneuron synapse. Neuron 18:1009–1023.

Gulyás AI, Miles R, Sík A, Tóth K, Tamamaki N, Freund TF. 1993. Hippocampal pyramidal cells excite inhibitory neurons through a single release site. Nature 366:683–687.

Hasselmo ME, Wyble BP. 1997. Free recall and recognition in a network model of the hippocampus: Simulating effects of scopolamine on human memory function. Behav Brain Res 89:1–34.

Hasselmo ME, Fehlau BP. 2001. Differences in time course of ACh and GABA modulation of excitatory synaptic potentials in slices of rat hippocampus. J Neurophysiol 86:1792–1802.
Hasselmo M, Schnell E, Barkai E. 1995. Dynamics of learning and recall at excitatory recurrent synapses and cholinergic modulation in rat hippocampal region CA3. J Neurosci 15:5249–5262.
Hasselmo ME, Bodelón C, Wyble BP. 2002. A proposed function for hippocampal theta rhythm: Separate phases of encoding and retrieval enhance reversal of prior learning. Neural Comput 14: 793–817.
Hefft S, Jonas P. 2005. Asynchronous GABA release generates long-lasting inhibition at a hippocampal interneuron—principal neuron synapse. Nat Neurosci 8:1319–1328.
Henze DA, Wittner L, Buzsaki G. 2002. Single granule cells reliably discharge targets in the hippocampal CA3 network in vivo. Nat Neurosci 5:790–795.
Hoskison M., Connor J., Shuttleworth C. 2004. GABAB-receptor modulation of short-term synaptic depression at an excitatory input to murine hippocampal CA3 pyramidal neurons. Neurosci Lett 365:48–53.
Hosseini-Sharifabad M, Nyengaard JR. 2007. Design-based estimation of neuronal number and individual neuronal volume in the rat hippocampus. J Neurosci Methods 162:206–214.
Hunsaker MR, Kesner RP. 2013. The operation of pattern separation and pattern completion processes associated with different attributes or domains of memory. Neurosci Biobehav Rev 37:36–58.
Ikonen S, McMahan R, Gallagher M, Eichenbaum H, Tanila H. 2002. Cholinergic system regulation of spatial representation by the hippocampus. Hippocampus 12:386–397.
Izhikevich EM. 2003. Simple model of spiking neurons. IEEE Trans Neural Netw 14:1569–1572.
Izhikevich EM. 2010. Dynamical Systems in Neuroscience: The Geometry of Excitability and Bursting. London: MIT Press.
Katona I, Acsády L, Freund T. 1999. Postsynaptic targets of somatostatin-immunoreactive interneurons in the rat hippocampus. Neuroscience 88:37–55.
Kim D, Paré D, Nair SS. 2013a. Assignment of model amygdala neurons to the fear memory trace depends on competitive synaptic interactions. J Neurosci 33:14354–14358.
Kim D, Paré D, Nair SS. 2013b. Mechanisms contributing to the induction and storage of Pavlovian fear memories in the lateral amygdala. Learn Mem 20:421–430.
Kitajima T, Hara K-I. 1997. An integrated model for activity-dependent synaptic modifications. Neural Netw 10:413–421.
Kosaka T, Katsumaru H, Hama K, Wu JY, Heizmann CW. 1987. GABAergic neurons containing the Ca2+-binding protein parvalbumin in the rat hippocampus and dentate gyrus. Brain Res 419:119–130.
Kremin T, Hasselmo ME. 2007. Cholinergic suppression of glutamatergic synaptic transmission in hippocampal region CA3 exhibits laminar selectivity: Implication for hippocampal network dynamics. Neuroscience 149:760–767.
Kunec S, Hasselmo ME, Kopell N. 2005. Encoding and retrieval in the CA3 region of the hippocampus: A model of theta-phase separation. J Neurophysiol 94:70–82.
Lawrence JJ, McBain CJ. 2003. Interneuron diversity series: Containing the detonation—Feedforward inhibition in the CA3 hippocampus. Trends Neurosci 26:631–640.
Lawrence JJ, Statland JM, Grinspan ZM, McBain CJ. 2006. Cell type-specific dependence of muscarinic signalling in mouse hippocampal stratum oriens interneurones. J Physiol 570:595–610.
Lee I, Kesner RP. 2004. Encoding versus retrieval of spatial memory: Double dissociation between the dentate gyrus and the perforant path inputs into CA3 in the dorsal hippocampus. Hippocampus 14:66–76.
Leutgeb JK, Leutgeb S, Moser M-B, Moser EI. 2007. Pattern separation in the dentate gyrus and CA3 of the hippocampus. Science 315:961–966.
Li G, Nair SS, Quirk GJ. 2009. A Biologically realistic network model of acquisition and extinction of conditioned fear associations in lateral amygdala neurons. J Neurophysiol 101:1629–1646.
Maccaferri G. 2005. Stratum oriens horizontal interneurone diversity and hippocampal network dynamics. J Physiol 562:73–80.
Maffei A. 2011. The many forms and functions of long term plasticity at GABAergic synapses. Neural Plast 2011:1–9.
Marr D. 1971. Simple memory: A theory for archicortex. Philos Trans R Soc Lond B Biol Sci 262:23–81.
Martin CB, Mirsattari SM, Pruessner JC, Pietrantonio S, Burneo JG, Hayman-Abello B, Köhler S. 2012. Déjà vu in unilateral temporal-lobe epilepsy is associated with selective familiarity impairments on experimental tasks of recognition memory. Neuropsychologia 50: 2981–2991.
McClelland JL, Goddard NH. 1996. Considerations arising from a complementary learning systems perspective on hippocampus and neocortex. Hippocampus 6:654–665.
McMahon DBT, Barrionuevo G. 2002. Short- and long-term plasticity of the perforant path synapse in hippocampal area CA3. J Neurophysiol 88:528–533.
McQuiston AR, Madison DV. 1999a. Muscarinic receptor activity has multiple effects on the resting membrane potentials of CA1 hippocampal interneurons. J Neurosci 19:5693–5702.
McQuiston AR, Madison DV. 1999b. Nicotinic receptor activation excites distinct subtypes of interneurons in the rat hippocampus. J Neurosci 19:2887–2896.
Meeter M, Murre JMJ, Talamini LM. 2004. Mode shifting between storage and recall based on novelty detection in oscillating hippocampal circuits. Hippocampus 14:722–741.
Miles R. 1990. Synaptic excitation of inhibitory cells by single CA3 hippocampal pyramidal cells of the guinea-pig in vitro. J Physiol 428:61–77.
Miles R, Wong RK. 1983. Single neurones can initiate synchronized population discharge in the hippocampus. Nature 306:371–373.
Miles R, Wong RK. 1986. Excitatory synaptic interactions between CA3 neurones in the guinea-pig hippocampus. J Physiol 373:397–418.
Miles R, Wong RK. 1987. Inhibitory control of local excitatory circuits in the guinea-pig hippocampus. J Physiol 388:611–629.
Misgeld U, Müller W, Polder HR. 1989. Potentiation and suppression by eserine of muscarinic synaptic transmission in the guinea-pig hippocampal slice. J Physiol 409:191–206.
Mizuseki K, Royer S, Diba K, Buzsáki G. 2012. Activity dynamics and behavioral correlates of CA3 and CA1 hippocampal pyramidal neurons. Hippocampus 22:1659–1680.
Naber PA, Caballero-Bleda M, Jorritsma-Byham B, Witter MP. 1997. Parallel input to the hippocampal memory system through peri- and postrhinal cortices. Neuroreport 8:2617–2621.
Neunuebel JP, Knierim JJ. 2014. CA3 retrieves coherent representations from degraded input: Direct evidence for CA3 pattern completion and dentate gyrus pattern separation. Neuron 81:416–427.
Newman EL, Gupta K, Climer JR, Monaghan CK, Hasselmo ME. 2012. Cholinergic modulation of cognitive processing: Insights drawn from computational models. Front Behav Neurosci 6:24.
Nolan CR, Wyeth G, Milford M, Wiles J. 2010. The race to learn: Spike timing and STDP can coordinate learning and recall in CA3. Hippocampus 21:647–660.
O'Reilly RC, McClelland JL. 1994. Hippocampal conjunctive encoding, storage, and recall: Avoiding a trade-off. Hippocampus 4:661–682.
Perry MA, Ryan CL, Tasker RA. 2009. Effects of low dose neonatal domoic acid administration on behavioural and physiological response to mild stress in adult rats. Physiol Behav 98:53–59.
Rogers JL, Kesner RP. 2003. Cholinergic modulation of the hippocampus during encoding and retrieval. Neurobiol Learn Mem 80: 332–342.
Rogers JL, Kesner RP. 2004. Cholinergic modulation of the hippocampus during encoding and retrieval of tone/shock-induced fear conditioning. Learn Mem 11:102–107.

Rolls ET, Kesner RP. 2006. A computational theory of hippocampal function, and empirical tests of the theory. Prog Neurobiol 79:1–48.

Royer S, Zemelman BV, Losonczy A, Kim J, Chance F, Magee JC, Buzsáki G. 2012. Control of timing, rate and bursts of hippocampal place cells by dendritic and somatic inhibition. Nat Neurosci 15:769–775.

Seress L, Pokorny J. 1981. Structure of the granular layer of the rat dentate gyrus. A light microscopic and Golgi study. J Anat 133: 181–195.

Shouval HZ, Bear MF, Cooper LN. 2002. A unified model of NMDA receptor-dependent bidirectional synaptic plasticity. Proc Natl Acad Sci USA 99:10831–10836.

Sik A, Penttonen M, Ylinen A, Buzsaki G. 1995. Hippocampal CA1 interneurons: An in vivo intracellular labeling study. J Neurosci 15: 6651–6665.

Staley KJ, Otis TS, Mody I. 1992. Membrane properties of dentate gyrus granule cells: Comparison of sharp microelectrode and whole-cell recordings. J Neurophysiol 67:1346–1358.

Sussillo D, Toyoizumi T, Maass W. 2007. Self-tuning of neural circuits through short-term synaptic plasticity. J Neurophysiol 97: 4079–4095.

Szabadics J, Soltesz I. 2009. Functional specificity of mossy fiber innervation of GABAergic cells in the hippocampus. J Neurosci 29:4239–4251.

Tóth K. 2010. Glutamatergic neurotransmission in the hippocampus. In: Cutsuridis V, Graham B, Cobb S, Vida I, editors. Hippocampal Microcircuits. New York: Springer. p. 99–128.

Toth K, Suares G, Lawrence JJ, Philips-Tansey E, McBain CJ. 2000. Differential mechanisms of transmission at three types of mossy fiber synapse. J Neurosci 20:8279–8289.

Traub RD, Miles R, Wong RK. 1987. Models of synchronized hippocampal bursts in the presence of inhibition. I. Single population events. J Neurophysiol 58:739–751.

Treves A, Rolls ET. 1992. Computational constraints suggest the need for two distinct input systems to the hippocampal CA3 network. Hippocampus 2:189–199.

Varela JA, Sen K, Gibson J, Fost J, Abbott LF, Nelson SB. 1997. A quantitative description of short-term plasticity at excitatory synapses in layer 2/3 of rat primary visual cortex. J Neurosci 17:7926–7940.

Vida I. 2010. Morphology of hippocampal neurons. In: Cutsuridis V, Graham B, Cobb S, Vida I, editors. Hippocampal Microcircuits. New York: Springer. pp 27–67.

Vogt KE, Regehr WG. 2001. Cholinergic modulation of excitatory synaptic transmission in the CA3 area of the hippocampus. J Neurosci 21:75–83.

Witter MP. 2010. Connectivity of the hippocampus. In: Cutsuridis V, Graham B, Cobb S, Vida I, editors. Hippocampal Microcircuits. New York: Springer. pp 5–26.

Wittner L, Henze DA, Záborszky L, Buzsáki G. 2006. Hippocampal CA3 pyramidal cells selectively innervate aspiny interneurons. Eur J Neurosci 24:1286–1298.

Wittner L, Henze D, Záborszky L, Buzsáki G. 2007. Three-dimensional reconstruction of the axon arbor of a CA3 pyramidal cell recorded and filled in vivo. Brain Struct Funct 212:75–83.

Woodin MA, Ganguly K, Poo M. 2003. Coincident pre- and postsynaptic activity modifies GABAergic synapses by postsynaptic changes in Cl- transporter activity. Neuron 39:807–820.

Woolf NJ. 1991. Cholinergic systems in mammalian brain and spinal cord. Prog Neurobiol 37:475–524.

Wyeth MS, Zhang N, Mody I, Houser CR. 2010. Selective reduction of cholecystokinin-positive basket cell innervation in a model of temporal lobe epilepsy. J Neurosci 30:8993–9006.